Hydrogeochemical processes after oxidation of sea sediment at mega-scale suppletion 'The Sand Motor'

Comparison between a mega scale suppletion site, a traditional suppletion site and a control site

Lieke Doodeman

Supervisors: Prof. Jasper Griffioen, MSc. Iris Pit

Utrecht, November 2013

Master thesis Sustainable Development, track Global change and Ecosystems, 45 ECTS

Cover photograph: The Sand Motor, January 2012 (Province of Zuid-Holland, 2013).

Universiteit Utrecht

Contents

Abstract

The Netherlands is a low-lying country, which is protected against flooding by the coastline. However, the coast is under threat by erosion and the predicted sealevel rise. Therefore, regular sand suppletion is performed to keep the coastal safety at reference level. Unfortunately, suppletion causes ecosystem disturbance. Consequently, the new paradigm 'Building with Nature' is developed, which promotes a more natural approach for coastal maintenance. An example of this is the Sand Motor, a megasuppletion pilot project constructed in sea between The Hague and Hoek van Holland. The application of $21*10^6$ m^3 of sea sediment will prevent suppletion for the next 20 years and the sand will be distributed over the coast by natural processes.

This research focusses on hydrogeochemical processes on the Sand Motor, since oxidation of former sea sediments can influence the soil and water quality. The mineral pyrite (FeS_2) is formed on the seafloor and is expected to dissolve in ground- and pore water upon oxidation. The sulphide mineral is of interest, because oxidation could acidify the groundwater and possibly mobilise adsorbed trace contaminants.

In order to evaluate whether geochemical processes may form a negative aspect of the Sand Motor, fieldwork was on performed on the Sand Motor, a traditional suppletion site and a control site. The groundwater and pore water samples were measured for alkalinity, ions, major elements and trace elements. Also, the carbon and sulphur contents of sediment samples were determined. The presence of pyrite on the Sand Motor was proven by Micro XRF and microprobing.

Soluble sulphate in combination with iron oxide confirms the oxidation of pyrite on the Sand Motor, but large-scale presence of pyrite is not proven. The oxidation effects are most prominent in the unsaturated zone in the middle of the Sand Motor where freshening has advanced the furthest. The buffering capacity is generally high, however, a selection of samples shows acidification or decreased alkalinity due to pyrite oxidation in the unsaturated zone. This results in trace elements exceeding target values and occasionally intervention values for shallow groundwater. The impact of pyrite oxidation on the traditional suppletion site is moderate. However, the control site indicates, contrary to expectations, more significant pyrite oxidation.

Long-term monitoring of the Sand Motor is recommended to see whether the elevated trace element concentrations are temporal or will persist for longer periods of time. Further monitoring will demonstrate whether pyrite oxidation is a hazardous aspect of the Sand Motor.

Chapter 1

Introduction

1.1 Coastal protection

The Netherlands is a low-lying country with a coastline of more than 400 km. Nine million people are living below sealevel and the majority of the gross domestic product is earned in these areas. The main function of the coast is the protection of the hinterland against flooding by the sea (Mulder et al., 2011). The IPCC warns that the current climate change and the corresponding sealevel rise will expose coasts to more risk. Consequences include an increase in coastal erosion (Alley et al., 2007). The Dutch coast is already prone to erosion, which, without human interference, would result into a retrograding coastline (Bakker et al., 2012). The necessity for coastal erosion management has grown even further by the expected increase in concentrations of people and economic values in the low-lying areas (Mulder et al., 2011). Additionally, the coastline provides ecological values, drinking water supply, recreation and residential functions (Oude Essink et al., 2010).

The ability of the coastline to protect the hinterland depends on the amount of sediment present, the type and distribution of sand over the coast. The coast is continually prone to changes by influence of the tides, waves, soil subsidence, rising seawater levels and river discharge (Stowa, 2013). On an erosional coast the beach forms a small buffer between the sea and the dunes. On a growing coast the beach has broadened forming a large buffer between the sea and the coastal strip, which are the dunes bordering the beach. Hence, the coastal strip is better protected and embryonic dune can form on the beach (Van der Sluis).

Coastal maintenance will restore the coastal safety when the local coastline does not meet the minimum safety demands due to for example erosion. Artificial sediment management is performed in order to keep the coastline at the 1990 position (Mulder and Tonnon, 2010), since the coastline of the year 1990 acts as the reference Coast Line (BCL). Sand suppletion is applied on the dunes, beach or foreshore when the BCL is exceeded, thereby increasing the total availability of sediment in the coastal system (Rijkswaterstaat, 2012a). The supplied sand is distributed along the coast by currents, wind and waves. Application of sand has

the preference over solid constructions, such as dams and dikes, since it causes a positive reinforcement over a larger area instead of increasing only the local safety (Stowa, 2013). The average annual nourishment volume was $6*10^6$ m^3 between 1990 and 2000. In 2001 suppletion volumes increased to $12*10^6$ m^3 $year^{-1}$, which was needed to compensate for the sealevel rise of 1.8 mm $year^{-1}$. However, a recent update of the sediment balance of the coastal foundation showed a nourishment shortage of $20*10^6$ m^3 (Mulder and Tonnon, 2010). The Delta committee, the governmental advice committee on water safety, therefore advises to battle sealevel rise by enforcing and improving the maintenance of the Dutch coast. According to the committee a raise of the yearly suppletion to $40*10^6$ - $85*10^6$ m^3 of sand in 2050 is required to protect the Netherlands against the predicted sealevel rise (Deltacommissie, 2008). Since the coastline will have moved between 100 and 400 m inland by 2100 without sand suppletion (Stronkhorst et al., 2011).

Four types of sediment suppletion exist. First, dune suppletion is applied when coastal protection needs immediate improvement because the local coastline does not meet the minimum security norms. Second, beach suppletion broadens the beach and moves the coastline seawards. Third, foreshore suppletion is the application of sand on the sea floor close to the coast at a depth of 5 to 8 meters. The sand forms a sandbar, from where the sand is transported towards the coast by the current. Foreshore suppletion does not have a direct effect, but reduces the negative effects of coastal erosion. Fourth, a megasuppletion is a new type of suppletion, which has been constructed only recently for the first time. It entails the single application of a large volume of sand for long term coastal safety. The sand is distributed in a natural way over the coast, thereby, after the initial start, decreasing the disturbance on the coastal ecosystems on the long term (Stowa, 2013).

The application of sand volumes is accompanied by disturbance of the natural processes and ecosystems. The ecology of the coastal system is to a great extent determined by morphological processes. Consequently, changes in the morphology in both time and space can result in changes in the ecosystem. The coastal zone consists of the surf zone, the wet and dry beach, the coastal strip and the dunes further inland. These habitats have their own ecological and morphological dynamics, but together they form the ecosystem of the coastal zone. Therefore, changes in one habitat can have an effect on the other habitats. First, dune suppletion can bury the vegetation and addition of a different type of sand can influence the geochemistry in the soil of the coastal strip, for example the calcium carbonate content. Second, beach suppletion affects the benthic animals. Third, the sea floor fauna and sea floor stability offshore are affected by the collection of sea sand for suppletion. Even though the redistribution of foreshore suppletion by natural processes lessens the impact on the system, the applied sand changes the morphology, increases sediment fluxes and possibly influences the reproductive function of the offshore zone (Holzhauer et al., 2009).

In order to protect the country against sealevel rise in a more environmentally friendly manner a new paradigm was developed called 'Ecological Engineering' or 'Building with Nature' (De Vriend and Van Koningsveld, 2012), which main

objective is to work with nature instead of against it. The new insights promote a natural approach which aims to prevent disturbance of ecological processes and ecosystems resulting in the maintenance of natural habitats. According to Mulder and Tonnon (2010) the adoption of natural processes offers the best chance of adaptation to climate change and it has the lowest costs on the long term.

1.2 The Sand Motor

The mega scale suppletion project the Sand Motor adopts the new approach 'Building with Nature'. The pilot is an example of large scale 'natural' shore nourishment. The Sand Motor is a peninsula constructed in 2011 between Hoek van Holland and the city The Hague (figure 3.1). The 128 ha plain was constructed in sea next to the beach using $21*10^6$ m^3 of sand. The Sand Motor is an innovative way of coastal protection, which aims to protect the hinterland from flooding by letting natural processes distribute sand over the shore face, beach and dunes (Mulder and Tonnon, 2010). It is envisioned that after the initial disturbance during construction the Sand Motor project will result in gradual and natural suppletion of the coastal zone (figure 1.1). Furthermore, dispersion of the Sand Motor sand by natural processes will not disturb the ecosystems and will create opportunities for recreation and nature development (Rijkswaterstaat, 2012c). Additionally, the expanded coast can lead to a freshwater supply in the peninsula (Technology Foundation STW, 2011). In the end, the applied volumes of sand should be sufficient to locally maintain the coast at the reference line for the next 20 years (Mulder and Tonnon, 2010).

The project will be monitored intensively since the Sand Motor is a pilot and the current state significantly differs from the original situation. The monitoring is expected to increase the knowledge of morphological, hydrological, geochemical, ecological and societal processes of mega nourishments. Also, the predictive capability regarding this type of shore nourishment will be enhanced. If the pilot is a success the new and more sustainable method could replace the current more disturbing methods of coastal suppletion. The assessment of the effectiveness of the nourishment can possibly lead to exportable technology (Technology Foundation STW, 2011).

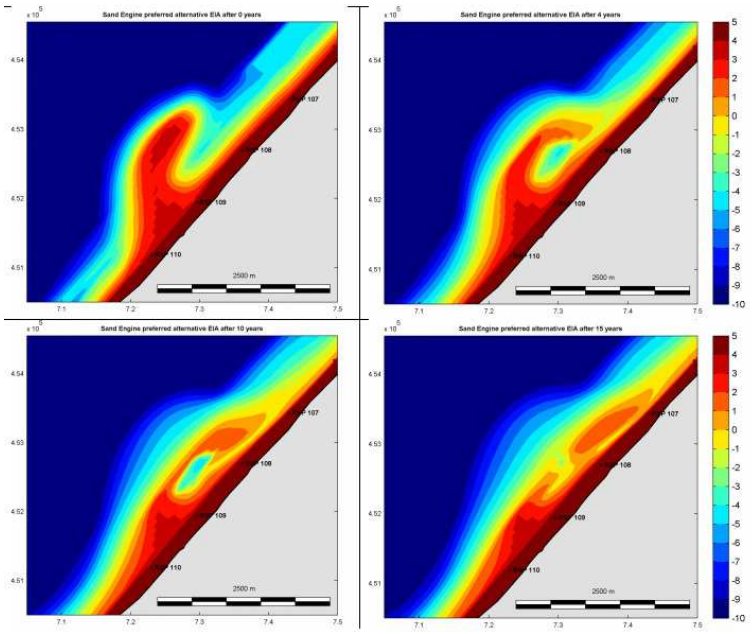

Figure 1.1: Computed morphological development of hook-shaped design with the initial shape in the upper left panel, and the development after respectively 4, 10 and 15 years from 2010 in the upper right, lower left and lower right panel , respectively (Mulder and Tonnon, 2010).

1.3 Research focus and objective

The monitoring of the Sand Motor will lead to knowledge on both the positive and negative consequences of a mega scale suppletion project. This research focuses on a small part of the different fields of study needed for the assessment, namely chemical processes on the Sand Motor. Chemical processes are an important component of the overall research, since the sand will be distributed over the shore face, beach and dunes, thereby spreading the possible chemical effects. The geochemical and mineralogical composition of the sea sand will affect the soil and water quality. Furthermore, possibly hazardous consequences of chemical processes can spread easily by infiltrating rainwater and groundwater flow. Additionally, the quality of a developing freshwater supply in the Sand Motor can be of interest for drinking water companies. Also, ecosystem succession in the dunes can be influenced (Technology Foundation STW, 2011). Therefore, gaining insight in the occurrence of the geochemical processes is important.

The calcareous sand used for the construction has been transported from the sea floor to the surface changing the conditions to an aerobic situation, thereby triggering biogeochemical processes. Stable minerals which were formed on the anoxic sea floor dissolve due to oxygenation processes, thereupon mobilising its mineral components. An example of a stable and widespread authigenic component of sea sediment is the mineral pyrite (FeS_2). The mineral is the most common sulphide mineral and is known to dissolve after oxidation. Pyrite and other metal-sulphide minerals have been studied intensively because of their importance for environmental quality (Evangelou and Zhang, 1995). The interest stems largely from the role adsorbed trace contaminants of the mineral play in anoxic coastal sediments. Pyrite is stable in the absence of air and in the presence of dissolved sulphide (Berner, 1984), conditions that occur on the sea floor. Thus, upon oxidation of former marine sediment the mineral dissolves. Consequently, possible impurities in the pyrite mineral are mobilised and the unwanted trace elements become a source of contamination. The mobilisation of toxic metals is an environmental hazard for the Sand Motor. A direct risk is the pollution of water used for recreation resulting in public health issues.

Since the Sand Motor consists of recently drained and exposed sediments the mineral pyrite is of immediate interest for the occurring chemical processes. Tuinenburg (2012) did the first orientating study concerning pyrite oxidation on the Sand Motor by analysis of the groundwater. He concluded that the sulphate/chloride ratio and alkalinity concentrations in groundwater and the presence of iron oxide indicated the possible occurrence of pyrite oxidation. However, the actual occurrence and scale of pyrite oxidation and contamination by trace elements was not proven by elemental analysis of the groundwater, pore water or sediment. Thus, this research focuses further on pyrite oxidation at the Sand Motor mega-nourishment.

This research aims to get insight in both the presence of pyrite and spatial distribution of pyrite oxidation in both the ground- and pore water. Another important

question is whether the mineral contains trace elements and if these elements pose a hazard for the environment due to mobilisation. Additionally, the groundwater is freshening simultaneously, moderating the effects of pyrite oxidation processes to an unknown degree. Finally, the goal is to assess whether pyrite oxidation processes are a harmful aspect of the megasuppletion.

In order to evaluate whether the geochemical processes on the Sand Motor may form a negative aspect of the project, fieldwork was performed on the Sand Motor. Additionally, two other coastal settings were studied in a similar manner. The first is a traditional suppletion site, which receives regular maintenance. The second location acts as a control site, where the beach grows without human interference. A comparison between the three sites can give insight with respect to the occurrence of pyrite processes and can quantify the presence of trace elements.

1.4 Hypothesis

1. Pyrite oxidation is expected to take place on the Sand Motor, since the megasuppletion is constructed of recently oxidised sea sediments. Additionally, the mineral pyrite FeS_2 is a common mineral formed on the sea floor. Pyrite dissolves upon oxidation, which will result in elevated SO_4^{2-} concentrations in both the pore and groundwater and possibly dissolved Fe^{2+}. The acidity produced by the oxidation is buffered by calcareous sand, which induces Fe^{3+} to precipitate as $Fe(OH)_3$. Consequently, the precipitate is visible as a red brown coating on sand grains.

    (a) Pyrite oxidation is anticipated to be most prominent on the Sand Motor compared to the traditional suppletion site and the control site, since suppletion here was large scale and took place recently. The pyrite oxidation process is less visible on a traditional suppletion site because the suppletion volume on an erosional coast is smaller, but likewise, the oxidation effects are also time dependant. Pyrite oxidation is not anticipated to have occurred on the control site consisting of natural beach and dunes since no direct suppletion has taken place there. Even though, natural beach growth is often enabled by eroded sand of suppletion beaches, the effects are predicted to be insignificant in comparison with the Sand Motor, because it is unlikely that the transported erosion sediments still contain pyrite minerals.

    (b) Pyrite oxidation is expected to be an active process in the tidal zone. Even though the pyrite oxidation in the unsaturated zone has perhaps already ceased due to continuous exposure to oxygen, the tidal zone can still experience pyrite oxidation delayed by the interchanging conditions of saturation and oxidation. Consequently, this results locally in high sulphate concentrations and precipitated iron oxide.

2. Calcite buffering is expected to have prevented acidification. Assuming the presence of trace elements in the pyrite, the release of potentially toxic cations in water is inhibited since the mobility of cations increases in acid environments. However, neutral pH can promote the solubility of other trace elements, the oxyanions, which remain mobile in neutral pH conditions, resulting in significant concentrations of those specific elements.

    (a) The buffering capacity is assumed to have decreased in the Sand Motor over the previous years causing the buffering capacity to be the lowest at the top of the unsaturated zone and the highest in the saturated zone. This is caused by the decrease of oxygen levels with depth which limits pyrite oxidation. Consequently, oxidation is expected to have advanced furthest in the unsaturated zone. However, overall the buffering capacity has not been depleted, since measurements in 2012 did not indicate such events (Tuinenburg, 2012; Deltares, 2012).

    (b) The impact of pyrite oxidation with respect to the buffering capacity is expected to be smaller on the traditional suppletion site and the control site. The suppletion volumes of a traditional suppletion are much smaller compared to the megasuppletion the Sand Motor. Therefore, the geochemical processes evoked by the application have a smaller impact and the effects cease earlier. Nonetheless, a decreased buffering capacity is also expected in the traditional suppletion sites since this sand was also retrieved from an anoxic sea floor. The buffer is sufficient to prevent the release of PTEs. However, the amount of Fe, As and trace elements will be higher at both suppletion sites compared to the control site since research of Stuyfzand et al. (2010) indicates that suppletion sand in general contains more trace elements. The natural growth of the control beach with calcareous sands will not have caused processes affecting the pH. Therefore, a high buffering capacity remains present due to the calcareous sands.

3. The Sand Motor aquifer is freshening, because it is constructed of sediments derived from the seafloor 10 km from the coast. Therefore, the peninsula formed a salt aquifer after construction. Since then infiltration of rainwater has been slowly freshening the groundwater. It is assumed that aquifer freshening caused cation exchange, which changes the dominant fresh groundwater element calcium for sodium. Consequently, calcite undersaturation stimulates calcite dissolution resulting in increased alkalinity levels, which counteracts the acidification after pyrite oxidation and increases the buffering capacity. Freshening processes can also occur on the traditional suppletion beach and control site, but on a smaller scale. The fresh/salt water divide on beaches can shift due to for example winter storms followed by calm weather in spring.

1.5 Report structure

The following chapter (chapter 2) gives background information on pyrite formation, pyrite oxidation, toxic elements and refreshing of an aquifer. In chapter 4 the method of research is explained. The three different fieldwork sites are described and the method of sample collection is clarified. Additionally, details of the laboratory analyses are demonstrated. In chapter 5 the results of the fieldwork on the Sand Motor, in Noordwijk and IJmuiden are presented. Furthermore, data from research of Tuinenburg (2012) and Deltares (2012) on the Sand Motor is shown. This is followed by the discussion in chapter 6. In the discussion the research questions will be answered and clarifications for and possible mechanisms behind the presented results are given. The final conclusions are drawn in chapter 7 and general recommendations for further research will be given.

Chapter 2

Chemical processes after suppletion

2.1 Pyrite formation

Pyrite formation can occur in different sedimentary settings, as aquifers, lakes, swamps and soils, but most pyrite is formed in marine coastal environments (Schoonen, 2004)). Pyrite (FeS_2), iron disulphide, is formed in an anoxic environment. Formation requires a continuous supply of sulphate and iron in the presence of easily decomposable organic matter. Pyrite formation in marine sediments compared to freshwater sediments is relatively rapid, since the sulphate concentrations are two to three orders of magnitude higher in sea water. Therefore, the major control on pyrite formation in marine sediments is organic matter (Evangelou and Zhang, 1995; Bierens de Haan, 1991).

Pyrite is formed by the transformation of iron monosulphides (FeS) to iron disulphide (FeS_2) during early diagenesis (Berner, 1984), since pyrite is thermodynamically the more stable iron sulphide phase. The mineral is stable over a large range of pe-pH parameter space in anoxic low-temperature environments (Schoonen, 2004; Wang and Morse, 1996). Sedimentary pyrite occurs as euhedral crystals, well formed grains with a distinct shape or as spheroidal aggregates, called framboids (Bierens de Haan, 1991).

Trace elements can be incorporated or adsorbed to the pyrite mineral and can consequently be released upon pyrite oxidation. The elements are included during the pyritization process, by which pyrite acts as a host mineral. The composition of pyrite differs as shown by various articles (Dorronsoro et al., 2002; Schoonen, 2004; Huerta-Diaz and Morse, 1990; Clemente et al., 2006; Rimstidt and Vaughan, 2003; Billon et al., 2001; Elbaz-Poulichet et al., 2000; Sohlenius and Born, 2004). The trace elements most mentioned are Mn, Cu, Pb, Zn, As, Sb, Se, Co, Cd, Hg, Cr and Ni.

The mechanism behind incorporation of impurities in pyrite is not yet fully clear given the complexities in the formation of the mineral. There are several

processes possible. First, when iron monosulphide is converted to pyrite, trace elements present in FeS will be incorporated in the pyrite (Schoonen, 2004). Second, some trace elements (e.g. Co, Cu, Zn) can form sulphide complexes in sulphidic waters and arsenic forms arsenic oxyanions. Both complexes can become adsorbed to surfaces on pre-existing pyrite crystals, thereby increasing the DTMP (Degree of trace metal pyritization values) (Scholz and Neumann, 2007). Finally, the mineral often experiences multiple stages of pyrite formation, which can influence the trace element composition of the iron disulphide. Thus, the trace elements become incorporated during the crystal growth (Schoonen, 2004).

2.2 Pyrite oxidation

Pyrite oxidation is an example of acid rock drainage (ARD) or acid mine drainage (AMD), which can either be a natural process or promoted by human activity, causing sulphide-bearing material to be exposed to oxygen and water. The generated acid water contains high concentrations of metals and other toxic ions (Akcil and Koldas, 2006). Metal sulphide minerals, of which pyrite is by far the most naturally abundant, are generally not stable in the earth's atmosphere, near earth's surface or when in contact with oxygenated water (Cotter-Howells et al., 2000). Oxidation of pyrite starts when the conditions change from an anoxic to an oxic environment. Such a change may occur when sand is removed from the sea floor or when a sea is drained to create land. Factors such as pH, P_{O_2}, specific surface and morphology of pyrite, presence or absence of bacteria, clay minerals, as well as hydrological factors determine the rate of oxidation (Evangelou and Zhang, 1995).

The oxidation of pyrite can act as a source of sulphate (SO_4^{2-}), Fe-oxides and heavy metals in the environment. All possible oxidation reactions are displayed in the schematic overview of figure 2.1. The overall reaction of pyrite oxidation by O_2 is shown by chemical reaction formula 2.1. This reaction can be separated into steps. The oxidation of disulphide (S_2^{2-}) to sulphate may be caused by the presence of O_2 (reaction 2.2 and pathway (a) in Figure 2.1) or by Fe^{3+} (reaction 2.3) and pathway (c)). This is followed by the oxidation of Fe^{2+} to Fe^{3+} (reaction 2.4 and pathway (b)), after which depending on the pH Fe^{3+} will precipitate as $Fe(OH)_3$ (reaction 2.5 and pathway (d)) (Appelo and Postma).

$$\mathbf{FeS_{2\,(s)}} + \frac{15}{4}\mathbf{O_{2\,(g)}} + \frac{7}{2}\mathbf{H_2O} \longrightarrow \mathbf{Fe(OH)_{3\,(s)}} + \mathbf{2SO_4^{2-}{}_{(aq)}} + \mathbf{4H^+} \tag{2.1}$$

$$\mathrm{FeS_{2\,(s)}} + \frac{7}{2}\mathrm{O_{2\,(g)}} + \mathrm{H_2O} \longrightarrow \mathrm{Fe^{2+}{}_{(aq)}} + 2\mathrm{SO_4^{2-}{}_{(aq)}} + 2\mathrm{H^+} \tag{2.2}$$

$$\mathrm{FeS_{2\,(s)}} + 14\mathrm{Fe^{3+}{}_{(aq)}} + 8\mathrm{H_2O} \longrightarrow 15\mathrm{Fe^{2+}{}_{(aq)}} + 2\mathrm{SO_4^{2-}{}_{(aq)}} + 16\mathrm{H^+} \tag{2.3}$$

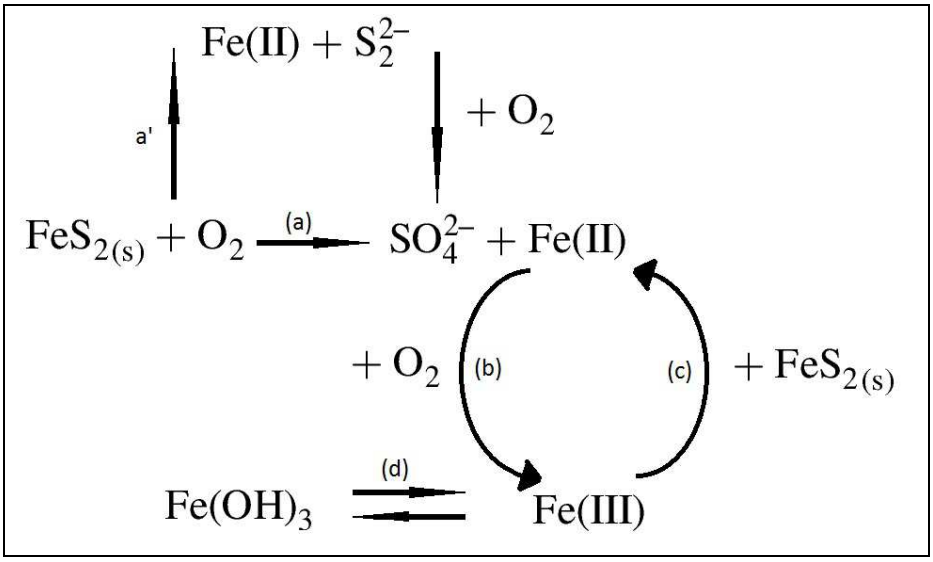

Figure 2.1: The reaction pathways in the oxidation of pyrite (Appelo and Postma)

$$\mathrm{Fe^{2+}}_{(\mathrm{aq})} + \frac{1}{4}\mathrm{O}_{2\,(\mathrm{g})} + \mathrm{H^{+}}_{(\mathrm{aq})} \longrightarrow \mathrm{Fe^{3+}}_{(\mathrm{aq})} + \frac{1}{2}\mathrm{H_2O} \tag{2.4}$$

$$\mathrm{Fe^{3+}}_{(\mathrm{aq})} + 3\mathrm{H_2O} \longrightarrow \mathrm{Fe(OH)}_{3\,(\mathrm{s})} + 3\,\mathrm{H^{+}}_{(\mathrm{aq})} \tag{2.5}$$

Precipitation of $Fe(OH)_3$ occurs at circumneutral pH when the solubility of Fe^{3+} is lowest. The precipitate may occur as an iron coating on remaining pyrite grains (Stipp et al., 2002). As a consequence, the iron oxide can strongly hinder the rate of pyrite oxidation due to physical transport through the oxide coating. The coating formation is prevented in environments which are sufficiently flushed with water (Andersen et al., 2001). The oxidation of pyrite-S by Fe^{3+} can take place in acid conditions due to high solubility (Cotter-Howells et al., 2000). This specific oxidation process is much more rapid than oxidation of pyriet-S by O_2 and oxidation of Fe^{2+} to Fe^{3+} by O_2. Therefore, reaction 2.4 is the rate-limiting step in the process, especially at low pH (Bierens de Haan, 1991).

The oxygenation reactions lead to the generation of acid solutions. However, the pH in former sea sediments is dominantly neutral due to the presence of calcium carbonate ($CaCO_3$). In carbonate soils, acidification and contamination of the soil is strongly limited due to the neutralizing effect of the calcite buffer on pH. The buffered pH inhibits transport of heavy metals. The $CaCO_3$ reacts with H^+ thereby neutralising the ion (reaction 2.6). This results into a increased alkalinity (HCO_3^-) levels in water (Dorronsoro et al., 2002). However, pyrite oxidation will decrease the pH when the buffering capacity is depleted (Andersen et al., 2001).

$$\mathrm{CaCO}_{3(\mathrm{s})} + \mathrm{H^{+}}_{(\mathrm{aq})} \longrightarrow \mathrm{Ca^{2+}}_{(\mathrm{aq})} + \mathrm{HCO^{-}}_{3(\mathrm{aq})} \tag{2.6}$$

2.3 Toxic elements

The breakdown of sulphide minerals releases major and minor elements. Incorporated trace elements can be mobilised upon pyrite oxidation and released in the environment. Elemental analyses of pyrite in coastal sediments often shows significant amounts of heavy metals and metalloids present in iron disulphide (Schoonen, 2004).

The trace elements mentioned in chapter 2.1 can be distinguished into two groups: the cations and oxyanions, which demonstrate different mobility and sorption behaviour (Schoonen, 2004). Arsenic is an anion and chromium and molybdenum are cations, but in solution all three form oxyanions. An oxyanion consists of a main element and an oxygen element according to the formula $A_xO_y^{z-}$ (Smedley and Kinniburgh, 2002). Research shows that the mobility of the oxyanions increases at circumneutral pH compared to acid conditions due to their alkaline characteristics. Chromium and molybdenum are mobile under oxidising conditions. However, the element arsenic can be mobilized under both reducing and oxidising circumstances, making it a problematic element in a wide range of environments (Smedley and Kinniburgh, 2002). Manganese, Zn, Ni, Pb, Cd, Cu and Co are cations, which are mobile in acid conditions and become more insoluble at near neutral pH. As a consequence the elements precipitate as, or co-precipitate with, an oxide, hydroxide, carbonate or phosphate mineral. Furthermore, the elements can experience adsorption to hydrous metal oxides, clay or organic matter (Smedley and Kinniburgh, 2002).

The transport or mobilisation of different contaminating elements in water is often hindered by secondary immobilization, which means adsorption or incorporation of the released elements to Fe-oxyhydroxides (for example $Fe(OH)_3$). The majority of the adsorbed elements (the cations) is released again at decreasing pH (Stipp et al., 2002), since the element adsorption to the surface of iron hydroxides is weakest at low pH when H^+ is competing for the sorption sites. The release of the different elements varies with the pH. At first Ni^{2+} starts the desorption with decreasing pH, this is followed by Zn^{2+}, Cd^{2+}, Cu^{2+}, Pb^{2+} and Cr^{3+}. Sulphate is more mobile since it is not sorbed in pH-neutral groundwater (Appelo and Postma). Arsenate (AsO_4^{3-}) and the other oxyanion-forming elements, however, become less strongly adsorbed at near-neutral pH (pH 6.5-8.5). The mobilisation of oxyanions at near-neutral pH compared to the behaviour of cations makes arsenic, chromium and molybdenum some of the most common contaminants in groundwater (Smedley and Kinniburgh, 2002).

The presence of the element arsenic leads to both environmental and health concern due to its high toxicity even at trace levels. Arsenic and other potentially toxic elements (PTEs), as Ni, Pb, Cd, Cu, Co, Cr and Zn, are naturally present in water, sediments and solids at trace levels (Rodrigues et al., 2010). The levels are often increased due to human disturbances, leading to a contaminated environment. The element concentrations become raised by oxidation of previously saturated anoxic sediments as a consequence of land drainage or beach suppletion

by sea sand (Roskam and Griffioen, 2011). Research by Stuyfzand et al. (2010) shows that suppletion sand contains more iron, arsenic and trace elements compared to natural dune sands. Undesired mobilization of trace elements depends on the concentrations in the mineral, oxidation levels and secondary chemical reactions (Roskam and Griffioen, 2011).

2.4 Freshening of an aquifer

The calcite buffering of acidification caused by pyrite oxidation can be enhanced by the process of aquifer freshening, which implies the relocation of the salt/fresh water interface. The composition of an initially marine aquifer can slowly change by infiltration of rain leading to a transition from a salt aquifer to a fresh water aquifer. When the groundwater composition changes also the chemicals of the solid phase must adapt to the new groundwater concentrations. The changing of the chemicals of the solid phase is referred to as the cation exchange (Appelo and Postma).

The dominant ions in seawater are Na^+ (sodium), Cl^- (chloride) and Mg^{2+}, accordingly sediment in contact with seawater will have Na^+ on the exchanger. The composition of coastal fresh groundwater is often dominated by Ca^{2+} (calcium) and HCO_3^-(bicarbonate), which result from calcite ($CaCO_3$) dissolution. The exchanger in fresh groundwater is occupied by Ca^{2+}. As a consequence reaction 2.7 occurs during aquifer freshening.

$$\frac{1}{2}\mathrm{Ca}^{2+} + \mathrm{Na} \cdot \mathrm{X} \longrightarrow \frac{1}{2}\mathrm{Ca} \cdot \mathrm{X}_2 + \mathrm{Na}^+ \tag{2.7}$$

The X indicates the sediment exchanger. Calcium is adsorbed and sodium is released, changing the water to a $NaHCO_3$ (sodium bicarbonate) watertype. This mechanism causes the groundwater to reflect aspects of its former composition even though the water quality is changing. When the aquifer gets flushed, the $Ca(HCO_3)_2$ (calcium bicarbonate) watertype returns. This water type appears more quicker along the more rapid flowlines or where the cation exchange capacity (CEC) is smaller. The adsorption of cations is largest on solid phases with large specific surface areas. Therefore, large grains are often coated with organic matter and iron oxyhydroxides, which prevent further adsorption of elements. As a consequence, the CEC depends on the clay content, clay minerals, organic matter and oxide or hydroxide content (Appelo and Postma).

Concluding, a surplus of sodium in the groundwater relative to the seawater can indicate freshening of the aquifer. The associated potassium and magnesium increase as well. The water becomes undersaturated for calcite after the calcium exchange for sodium, which results in dissolution. Calcite dissolution causes a significant increase in calcium and bicarbonate in the $NaHCO_3$- water. The alkalinity increases, since bicarbonate is the main component of alkalinity at circumneutral pH. The alkalinity can mount up to 10 mmol/l. Additionally, the dissolution affects

the pH of the $NaHCO_3$-water, which may increase to above 8. Furthermore, the sulphate and chloride concentrations in fresh water are lower than in marine water (Appelo and Postma).

Chapter 3

Study sites

Fieldwork was performed at three locations (figure 3.1) in order to answer the proposed research questions. The first is the novel and large-scale suppletion site the Sand Motor. The second is the beach of Noordwijk, where the erosional coast requires sand suppletion every few years. The third location is the beach of IJmuiden, which, shielded by the piers, continues to grow by natural processes. The calcite content of 1-5% (between Hoek van Holland and Bergen) is high compared to the other Dutch beaches and dunes (Stuyfzand et al., 2010).

Figure 3.1: The fieldwork locations IJmuiden, Noordwijk and the Sand Motor

3.1 The Sand Motor

The first fieldwork location is the Sand Motor (location 1), a sand plain of 128 ha. This hook-shaped mega-nourishment was constructed in 2011 with $21*10^6$ m^3 sand from the North Sea floor. Additionally, the project entailed broadening of the beach and the construction of a new dune line. Its maximum height is around 5 m above average sealevel in the middle of the plain. A lake is present at the south side of the Sand Motor. The slufter is the sea inlet at the northern side. In the future, the hook of the Sand Motor shall grow in northern direction and connect with the beach, after which in time a shallow plain shall form (figure 1.1). The sand will be distributed over the shoreface, beach and dunes by natural processes, which, according to the predictions, will heighten and increase the beach and dune area with 33 ha in 2031. The Sand Motor will enable the coastal foundation of Delfland to grow along with the expected sea level rise during the next 20 years (Mulder and Tonnon, 2010).

Since the construction of the Sand Motor, changes have been observed. The first pioneer plants and embryonic dunes have appeared on the Sand Motor. The salinity of the inner lake is changing from salt towards fresh (Tuinenburg, 2012). The morphology of the slufter has been narrowing, which can cause strong tidal currents. New slufter entries are forming and continue to move towards a northern direction abandoning former entries. The western seaside has a steep erosional wall of up to 1.5 m. The changing morphology recorded by aerial photographs can be seen in figures A.1 and A.2 of appendix A.

Groundwater measurements have been taken on the Sand Motor by Tuinenburg (2012) in spring 2012 and by Deltares in September 2012 (Deltares, 2012) (figure

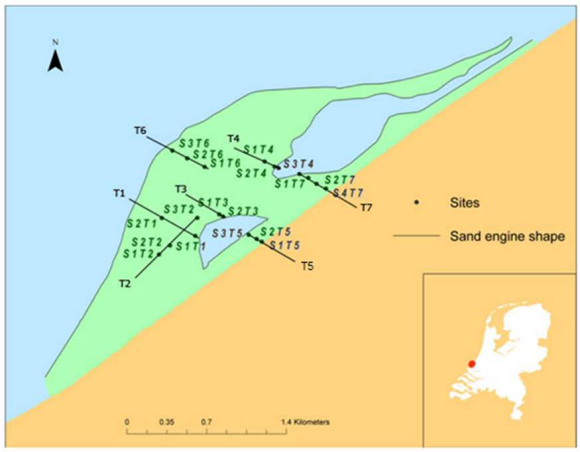

Figure 3.2: The groundwater sampling points of Tuinenburg (2012) on the Sand Motor taken in March and April 2012. Deltares partially repeated the measurements in summer 2012, they were mainly concentrated at the beach side of the Sand Motor.

3.2). A selection of these points were revisited to collect groundwater, pore water and sediment samples. The selection was based on previously interesting measurements, a good distribution over space and a good division between of locations in the middle of the Sand Motor and close to water. In total 10 drilling locations, the lake and the sea inlet were sampled. The chosen and renamed locations are shown in table 3.1 and figure 3.3.

Table 3.1: Renaming of the 2012 Sand Motor sampling points.

Sample name 2012	Sample name 2013
S2T3	B1
S3T2	B2
S3T8	B3
S1T6	B4
S3T6	B5
S2T8	B6
S2T7	B7
S2T4	B8
S1T4	B9
S1T8	B10

3.1.1 Previous Sand Motor measurements

Groundwater measurements have been taken at the Sand Motor by Tuinenburg (2012) in spring 2012. The results are summarized in tables 3.2 and 3.3.

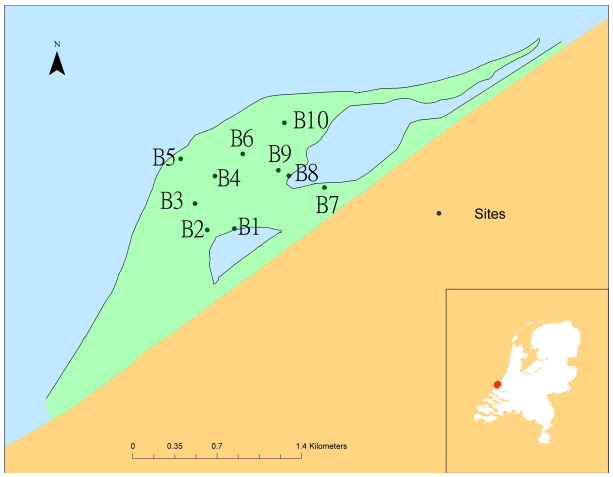

Figure 3.3: The sampling points of this research on the Sand Motor. Additionally the sea slufter and the lake were sampled. B6 and B7 were only measured for groundwater.

Sample name	Sample name	EC	pH	GW depth	Cl	SO_4^{2-}	Excess SO_4^{2-}	FeS_2 oxidation	Alkalinity
2012	2013	mS/cm		m	mmol/l	mmol/l	mmol/l	mmol/l	mmol/l
S2T3	B1	37	7.90	0.40	371.57	19.47	0.47	0.24	3.62
S3T2	B2	3	8.27	3.75	9.62	4.34	3.72	1.86	16.82
S1T6	B4	3	8.81	2.75	5.64	1.67	1.25	0.63	8.26
S3T6	B5	43	8.03	1.30	451.11	24.31	1.27	0.64	2.73
S2T7	B7	41	-	0.40	335.06	17.57	0.43	0.22	3.61
S2T4	B8	47	7.79	0.30	472.81	25.13	1.00	0.50	2.68
S1T4	B9	33	7.67	-	327.45	16.85	0.09	0.05	3.37
Lake	Lake	32	8.51	-	332.86	17.54	0.51	0.26	3.70
Sea	Slufter	43	8.06	-	438.39	22.98	0.59	0.26	2.70

Table 3.2: Sand Motor fieldwork data of groundwater as measured by Tuinenburg (2012). Only the locations re-sampled in 2013 are displayed.

Table 3.3: Trace elements in groundwater in μg/kg from Tuinenburg (2012) of overlapping sampling locations. The $\pm$ sign means that the measurements were below detection limit and no accurate concentration can be indicated. Max represents the target value for shallow groundwater (Staatscourant, 2012).

Sample	As	Ba	Co	Cr	Cu	Fe	Mn	Ni	Zn
Max	10	50	20	1	15	-	-	15	65
Detection limits	0.18	3.00	0.30	0.50	0.60	30	0.70	0.30	8.00
B1	15.9	66.6	12.5	3.9	6.1	37.1	466	21.7	180
B2	18.5	3.9	0.8	0.6	3.6	$\pm$0	0.8	3.4	20.7
B4	12.9	3.9	0.8	0.6	2.7	46.0	6.4	5.9	11.9
B5	18.7	6.3	1.9	4.8	9.3	1447	51.9	5.3	83.3
B7	13.2	17.7	5.2	3.4	2.0	$\pm$0	4.5	1.4	140
B8	27.8	33.0	7.6	4.6	4.8	$\pm$0	15.7	9.7	43.8
B9	2.6	2.1	0.6	0.8	2.3	$\pm$0	0.9	4.5	15.8

3.2 Noordwijk

The second location is Noordwijk aan Zee (location 2), which receives traditional suppletion to compensate for erosion (figure A.3 of appendix A). The required sand is obtained from the sea floor. The coastline and dune area near Noordwijk aan Zee are considered a weak link in the Dutch coastline, which means that the coastline that does not meet the minimum demands as described in the Dutch Waterlaw. Therefore, large foreshore suppletions were carried out in 1998, 2002 and 2006. However, Noordwijk aan Zee remained a weak spot, therefore project 'Dijk in Duin' was carried out from October 2007 until March 2008 along 1.5 km of the Noordwijker beach (Ruessink et al., 2012). The suppletion was coordinated with reference to the Jarkus row 8075-8525. Jarkus rows are coast profiles which are measured each year to map the coastal changes. The project entailed the restructuring of a small and narrow dune row into a wider and higher dune field. A 1.1 km long, 9 m high dike was built within the new dune. Furthermore, the beach was nourished alongshore over a length of 3 km with $3.0*10^6$ m^3 of sand. The suppletion pushed the low water line 40-50 m seawards and re-established the 1990 coastline. The project enabled the coastline to withstand a storm surge which occurs once every 10.000 years (Ruessink et al., 2012). A new beach suppletion of 250.000 m^3 is planned for 2013 (Rijkswaterstaat, 2012b).

In Noordwijk groundwater was sampled along three transects stretching from the dunes towards the shoreline. Transect 1 was also sampled for sediment and pore water.The locations of the transects were chosen in reference to the beach poles (number 80.0 and 80.25). In total 9 drilling locations divided over 3 transects were measured (figure 3.4.

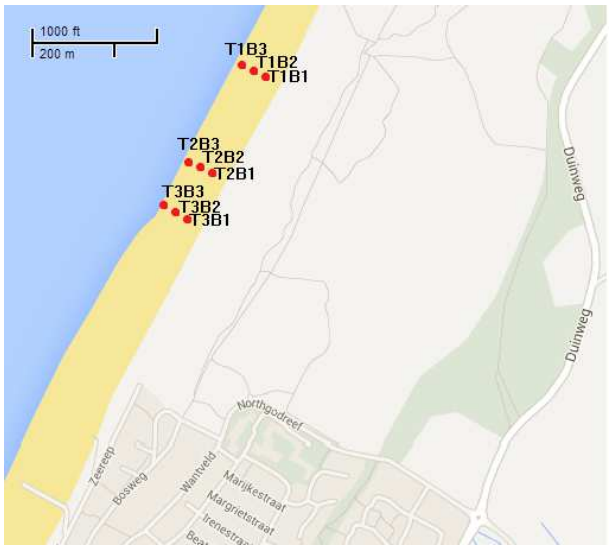

Figure 3.4: The sampling points of this research on the beach of Noordwijk aan Zee (the village visible south of the fieldwork location).

3.3 IJmuiden

The last location is the IJmuiden beach south of the south pier (location 3). The beach has been expanding since the first pier was built after the construction of the North Sea channel in the 19th century. The north and south pier were elongated in the 1960s, further promoting beach expansion (figure A.4a of appendix A). The older beach is now cultivated with the construction of a marine port, a boulevard and a lake. The sand from the Kennermermeer lake was used to construct dunes at the west and south side of the lake. The dune valley and the lake have developed in a very diverse nature area with reappearing plant species which had disappeared 100 years earlier due to water abstraction in the dunes. South of the dune valley a slufter, an opening in the dunes created by high tides, is present, but the development of small dunes continues to close the slufter (Landschap Noord-Holland, 2013). The nature development on the Kennemer beach has resulted in its selection as a Natura 2000 location. Currently, the beach shielded by the south pier continues to grow each year, which provides opportunities for embryonic dune development (figure A.4b of appendix A) (Natura2000, 2013). The sand is transported by sea currents from eroding beaches further south, which are receiving regular suppletion. As a result, suppletion is not needed. Therefore this location acts as a control site.

The active change in morphology on the beach near the pier could easily be seen in the winter and spring of 2013. In January the beach was flattened, probably by high tides and storms. Storm debris lay close to the dunes. However, three months later the debris had facilitated small dune formation. Dry sand had accumulated by the wind at the south side of the pier and bare dunes of up to 0.5 m

Figure 3.5: The sampling points of this research on the beach of IJmuiden.

were formed.

Samples at the beach of IJmuiden were taken on two places. The first location was on the beach directly next to the pier. The second location was near an old sea inlet, 1750 m south of the pier. At both locations two transects were established, all directed from the dunes towards the sea. A total of 14 drillings divided over 4 transects were made for groundwater sampling (figure 3.5). Transects 1 and 3 with an additional point closer towards sea and point T4B1 close to the dunes were also sampled for sediment and pore water.

Chapter 4

Methods

4.1 Sample collection and field measurements

First, the groundwater was sampled at all locations during March 2013. A hole was augered until the saturated zone was reached. A piezometer with filter piece and additional filter sock was placed in the saturated zone. The groundwater was extracted with the use of a peristaltic water pump and a polyethylene tube. The water was sampled after a minimum of 4 litres was extracted from the hole and the measured oxygen level had stabilized. Figure 4.1 gives a schematic overview of the drilling method.

The water was measured directly in the field for oxygen levels. Two bottles were filled for groundwater analysis after filtration with a 0.45 μm filter. The nalgene bottle was acidified with 10 μl/ml of HNO_3. The 60 ml bottle contained 600 μl HNO_3. The acidified sample was used for elemental analysis. The 20 ml glass bottles were filled completely, without air bubbles, with groundwater for measurement of alkalinity and for ion chromatographic analysis. Finally, a third glass bottle was filled without additional filtration. At the end of the field day the water in the bottle was measured for electric conductivity and pH. These measurements were done at the end of the day since the cold temperatures prevented quick stabilisation of equipment. The groundwater samples were kept cool overnight. After sampling the bore location was carefully located by a DGPS for sediment sampling and re-measurement in the future. However, the DGPS was not always available, in that case the drilling locations were located by a Garmin eTrex GPS and a description of the location with photos was made.

Second, the sediment samples were collected in the month of April and the first week of May (2013). They were taken to determine the presence and composition of pyrite and the composition of the pore water. A selection of groundwater sampling locations was revisited for sediment sampling. The amount of sediment sampling was limited by the number of sediment cores that could be processed the following day in the laboratory and the days available for fieldwork. The selection was based on the excess of sulphate present in the groundwater which could be

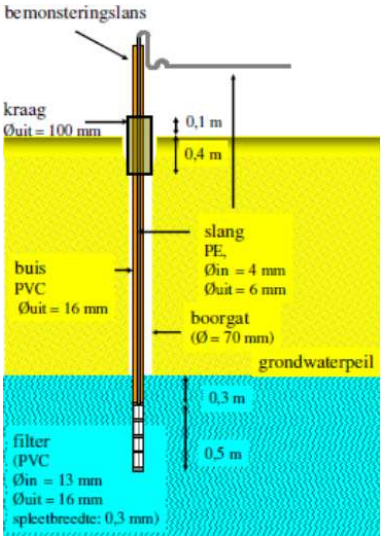

Figure 4.1: Schematic representation of groundwater sampling. The image gives indications of the size of the borehole, equipment and depth (in Dutch).

caused by pyrite oxidation.

The sediment cores were collected with an akkerman core sampler. The akkerman takes soil samples in stainless steel cores of maximum 20 cm long with a diameter of 38 mm. The sampler is hammered in the soil, leaving the soil relatively undisturbed (Eijkelkamp, 2013). The sampling depth for the sediment cores was determined by the groundwater depth as measured during groundwater sampling. The depth of the unsaturated zone determined the amount of samples taken at a specific location; 2, 3 or 4 samples. In case of two samples, the unsaturated and saturated zone were sampled. In case of three samples, one sediment sample was taken in the unsaturated zone, a second sample was taken in the tidal zone and the third in the saturated zone. In case of four samples, an additional sample was taken in the unsaturated zone. This method was applied to study whether the different oxygen levels might influence the composition of the water and sediment. The sediment sample from the tidal zone was taken when the sand became significantly wetter. In the unsaturated zone, and occasionally in the tidal zone, two cores would be collected per sampling depth in order to guarantee a sufficient amount of pore volume to perform all the analyses. The additional cores were taken at corresponding depth in a second auger hole 0.5 m from the original hole. Cores taken in the saturated zone were preferably closed with stainless steel fill-up pieces and plastic caps. The cores from the unsaturated zone were either closed with a plastic fill-up piece or aluminium foil under the plastic caps. At the end of the day the samples were stored in the refrigerator at a temperature of around 4 °C. The sediment was removed from the cores in the laboratory the following day.

A schematic overview of the sampling in depth is shown in figure 4.2 and the amount of samples divided per location is shown in table 4.1. The amount

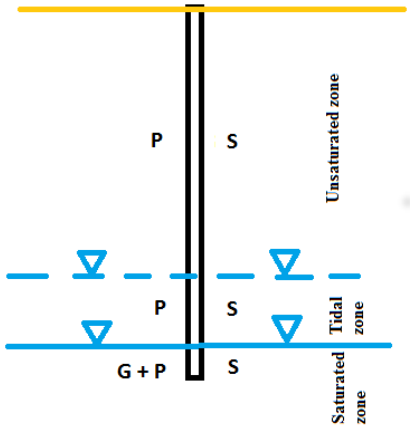

Figure 4.2: Schematic overview of the different samples in depth. The P represents sediment samples for pore water measurements, the S stands for sediment samples and the G stands for groundwater samples.

of samples taken on the Sand Motor is based on the estimation that 10 sampling locations evenly spread over the peninsula will result in a representative image of the spatial variability. In IJmuiden two locations of interest were selected. At both locations two transects were sampled. The assumption was made for Noordwijk that the beach was relatively uniform, therefore three transects seemed sufficient.

Table 4.1: The number of sampling points per field location

	The Sand Motor	Noordwijk	IJmuiden	Total
Transects	random	3	4	-
Sampling points	10	9	14	31
Groundwater samples	10 + 2 extra	9	14	31
Pore water samples	29	10	28	67
Sediment samples	29	10	28	67

4.2 Laboratory protocol

4.2.1 Pore water extraction

The sediment was extracted from the cores the day after sampling either by a sample extruder or by plastic spoon. Both the top and the bottom were discarded to avoid oxidised material. The pore water was extracted from the sediment by centrifuge. The sediment was placed in plastic home-made centrifuge bottles with a

0.45 μm filter at the bottom. The bottles received a plastic foil cover to prevent contamination from the centrifuge machine, limit oxidation of the sand and to keep the top and bottom of the bottle together. The sediment was centrifuged for 30 minutes at a speed of 2000 turns per minute.

First, the IJmuiden pore water from transect 1 was collected in the original plastic centrifuge buckets, which were rinsed with demi water. The samples for the IC, ICP and Gran method to determine alkalinity were taken with a syringe and 0.45 μm filter, since some centrifuge bottles allowed sediment to enter the sampling buckets underneath. The syringe was rinsed with demi water and reused. However, when the pore water yield was small, water for the different analyses was distributed by pipet, which prevented additional filtration. Second, the pore water from IJmuiden transect 3 was collected in Nalgene cups that were placed in the buckets and which were rinsed with acid (67-69% HCl), demi water and UHQ water. During the remaining sampling occasions, the water was sampled with fresh syringes and filters or pipets. Third, the pore water from Noordwijk and the Sand Motor was collected in the Nalgene cups with a cap on top, which prevented contamination of the collected pore water of the earlier mentioned sediment. Both were rinsed with HCl acid, demi water and UHQ water. Alkalinity and ion chromatography analyses were given priority when an insufficient amount of pore water could be extracted.

Finally, more than 1.5 ml of water was needed to test samples for elemental analysis by the ICP-MS and ICP-OES.

4.2.2 Water analysis

The day after sampling the non-acidified groundwater samples were tested manually for alkalinity by the GRAN method. The complete Gran method is added in appendix A. One or two ml of water sample was needed to determine the alkalinity.

Non-acidified water samples were measured on the Dionex DX-120 for the concentration of Cl, Br, NO_3, SO_4 and F. The testing required 2 ml of sample. The results have an uncertainty of 5%. The aim was to measure the day following the fieldwork. However, the anion analysis took place 2, 4 or 6 days later on a few occasions.

Acidified water samples were collected and measured in one serie. The ICP-OES measurement took place at the end of May. The water was analysed for Al, B, Ba, Be, Ca, Cl, Co, Cr, Cu, Fe, K, Li, Mg, Mn, Mo, Na, Ni, P, Pb, S, Sc, Si, Sr, Ti, V, Y, Zn and Zr. A selection of samples were further diluted to get a correct concentration of Ca, Cl, K, Mg, Na and S. ICP-MS measurements occurred at the end of June. The samples were analysed for Li, Be, Al, Sc, V, Cr, Mn, Fe, Co, Ni, Cu, Zn, Sr, Y, Zr, Mo, Cd, Ba, Pb and U. Unfortunately, not all pore water samples rendered enough water to permit measurement by the ICP.

It appears that during measurement of the groundwater and pore water of the Sand Motor on the Dionex DX-120 samples have been switched. The Dionex data for samples B3, B4, B5 and B6 and B9S1 and B9S2 did not correspond with the

ICP-OES data. The mistake was noted due to large difference in the chloride and sulphur concentration between the IC and ICP-OES results and the fact that the chloride levels did not match the EC field measurements. Additionally, when the Na/Cl and K/Cl ratios were calculated using IC chloride concentrations, significant outliers were present. Therefore, the Dionex data of B3, B4, B5 and B6 became B6, B3, B4 and B5 respectively. B9S1 and B9S2 were switched.

A selection of pore water samples of Noordwijk for the Dionex DX-120 were lost due to an accident in the laboratory. A more complete set of data could be constructed by combining both IC and ICP-OES data. However, three ICP-OES chloride measurements were above maximum detection limits, therefore, also the reconstructed dataset partially contains uncertainty.

Limitations of the data provided by the ICP-MS must be noted. The water samples were measures using a calibration line for samples with higher concentrations. Therefore most samples plotted underneath the lowest point of the calibration line rendering inaccurate measurements. As a consequence, for example, a concentration stating 0 μg/kg, can in reality have a concentration of 10 μg/kg. The trace element sample of Tuinenburg (2012) were measured with lower calibration line. Therefore the results for some elements seem higher, but this is not necessarily true. For this reason the detection limits have been added to all result tables. The detection limit is calculated by the limit of quantification (LOQ) times the sample dilution (20 times). The LOQ consists of 10 times the standard deviation.

4.2.3 CS analyses

The total carbon and sulphur contents were determined in the sediment which was collected for pore water extraction. First, the sediment was dried in the oven for 24 hours at a temperature of 104 °C. Then, the sediment was grinded. An average amount of 0.2 g of sediment was weighted in a small cup. The following day, the sediment was analysed with the CS analyser at a temperature of 1350 °C. The results gave the C and S content in % of the measured amount.

The results were lower than expected, therefore the process was repeated for three random samples. During the second round of measurements an accelerant was added to increase the temperature in the CS analyser. This would burn the sulphur possibly still incorporated in the sediment. However, the new measurements did not differ from the original ones.

The measured sulphur comprises both organic and inorganic S. Roskam and Griffioen (2011) determined the inorganic sulphur by assuming that all carbon present is organic and that the ratio of C/S is 100:1 in organic material. Thus, the excess of sulphur is expected to be inorganic and therefore possibly derived from pyrite.

For this research, the method is adjusted since a large part of carbon in beach sediments is derived from carbonates. Therefore, the minimum carbon content per location is assumed to indicate the carbonate content, which means that C_{min}=$C_{carbonate}$. The carbonate content as indicated by the minimum carbon content is 3.76% for

the Sand Motor, 3.16% for Noordwijk and 6.17% for IJmuiden. The method of Roskam and Griffioen (2011) is again applied after correction.

4.2.4 Micro XRF and microprobe

Two locations on the Sand Motor, based on the results of the CS measurements, were chosen to test for the presence for pyrite. The restriction to two samples was necessary due to the expensive and time-consuming analysis method. Samples B3S4 and B10S4 showed the highest content of inorganic sulphur. Consequently, these two samples were freeze-dried. Then, a selection of dominantly dark grains was made with the microscope for both samples. This was placed on a glass plate with tape. The sediment was analysed with the micro XRF for the presence of 16 elements: Al, As, Ca, Cr, Cu, Fe, K, Mg, Mn, Na, Ni, P, Rb, S, Si and Ti. The program EDAX image utilities analysed the results by mixing three elements. The grain colors of the resulting image correspond to the element content. The presence of pyrite was detected by the mixing of Fe and S, which resulted in a green/yellow color.

The grains which indicated the presence of pyrite, were selected and placed on another small plate, after which these were dried and placed in the microprobe. The microprobe can focus on individual grains and a beam can measure the elements present on a small patch of the grain. Consequently, when an element molar ratio Fe/S of 1:2 was measured the grain was considered pyrite.

4.3 Data analysis

4.3.1 Sulphate excess

The amount of sulphate in groundwater and pore water mainly depends on the mixing of freshwater with seawater. Equation 4.1 calculates the mixing ratio with the chloride concentrations in the water. The standard chloride content used for North Sea water was according to Van Wirdum (1991) and for rainwater according to Stolk (2001). The mixing ratio presented in equation 4.2 was used to calculate the corresponding sulphate concentration.

$$f_{seawater} = \frac{m_{Cl,sample} - m_{Cl,fresh}}{m_{Cl,sea} - m_{Cl,fresh}} \tag{4.1}$$

$$m_{i,mix} = f_{sea} \times m_{i,sea} + (1 - f_{sea}) \times m_{i,fresh} \tag{4.2}$$

When more sulphate is present than can be expected based on the mixing ratio, another sulphate source such as pyrite oxidation may be the cause. The possible excess of sulphate is calculated by subtracting the expected concentration from the measured sulphate concentration. After converting the units to mmol/l, the concentration is divided by two to estimate the 'calculated pyrite oxidation' in mmol/l.

The calculated excess of sulphate and alkalinity were assumed to be correlated. The data was organized in increasing levels of sulphate in order to see whether alkalinity would decrease with increasing sulphate concentrations, since this would be an indication of pyrite oxidation.

4.3.2 Mixing ratios

The ICP-OES measurements were compared with the mixing line to check for the presence of strange outliers or natural deviations. The mixing line indicates the expected concentrations of elements based on the mixing between fresh water and seawater. When the samples showed a clear inclination to plot below or above the mixing line, instead of on top, an explanation is needed. A similar mixing line was calculated for alkalinity. The standard composition of freshwater was taken from Stolk (2001). The composition of seawater was derived from Van Wirdum (1991).

4.3.3 PHREEQC

The saturation state for different minerals was calculated using the chemical program PHREEQC. The input data consisted of the concentration of pH, alkalinity, Cl, SO_4, Na, Mg, Al, K, Ca, Mn and Fe. The saturation indices of CO_2, Calcite, Dolomite, Gypsum, Fluorite, Siderite, Rhodochrosite, Quartz, Goethite and Hematite were calculated. Gypsum $CaSO_4 \cdot 2\,H_2O$ can form due to oxidation of sulphides (for example pyrite), after which the produced acid reacts with calcite. Calcite saturation is caused by dissolution of calcite.

Furthermore, an attempt was made to model the measured iron, sulphate, pH and alkalinity levels with PHREEQC. The script included seawater mixing ratios, pyrite oxidation, a simple cat-ion exchange followed by calcite addition, but this could not model the results found during fieldwork. Therefore, the model will not be considered any further.

4.3.4 Iron/iron oxide ratio

The ratio of soluble iron/iron oxide was calculated by using the sulphate excess. The sulphate indicated the amount of iron released after pyrite oxidation. This expected amount was compared with the measured amount of soluble iron, consequently, the percentage of precipitated iron was calculated.

Chapter 5

Results

5.1 Sulphate excess

The occurrence of pyrite oxidation is suggested by several indicators. To begin, the first indicator is the presence of more sulphate in the pore and groundwater than can be expected based on the mixing of fresh and salt water.

Figures 5.2a and 5.2b show the sulphate concentrations in relation to chloride in the ground- and pore water of the Sand Motor. Figures 5.4 and 5.3 display the situation in Noordwijk and IJmuiden respectively. When the data points appear above the mixing line, an excess of sulphate is present in the water. It is clear that both groundwater samples and pore water samples from the Sand Motor display an excess of sulphate. The excess amounts of the Sand Motor samples are the highest, compared to IJmuiden and Noordwijk. After the Sand Motor, IJmuiden shows the highest sulphate enrichment. Considering 5% measurement error, the excess of sulphate concentrations in the high chloride range have the highest uncertainty. However, data points which differ significantly remain above the mixing line. Also, the low chloride concentration samples are hardly affected by the 5% error, thus an excess of sulphate in the fresh water range is more certain.

The Sand Motor has a few points of interest with respect to high concentrations of excess sulphate (figure 5.1). For example, the groundwater of B3 has a calculated pyrite oxidation of 0.89 mmol/l at a mixing ratio of 0.11 (fraction of seawater f_{sw}, 11% seawater and 89% fresh water). Furthermore, the pore water measurements of B5 and B10 showed the highest calculated pyrite oxidation of respectively up to 1.36 and 1.49 mmol/l at a f_{sw} of 0.71 and 0.00. B6 and B7 were not remeasured for pore water testing. In general, pore water samples taken at larger depth resulted in a higher extent of pyrite oxidation. 2012 data indicates B2 as a point of interest due to high calculated pyrite oxidation (table 3.2 and figure 5.12). Therefore, detailed data of B2 amongst B3 and B10 is displayed in table 5.1.

The sulphate levels on the Noordwijker beach show lower pyrite oxidation, since the maximum excess concentration in the groundwater is 0.21 mmol/l at a f_{sw} of 0.01 (T1B1). Few data on pore water is available due to an accident in the

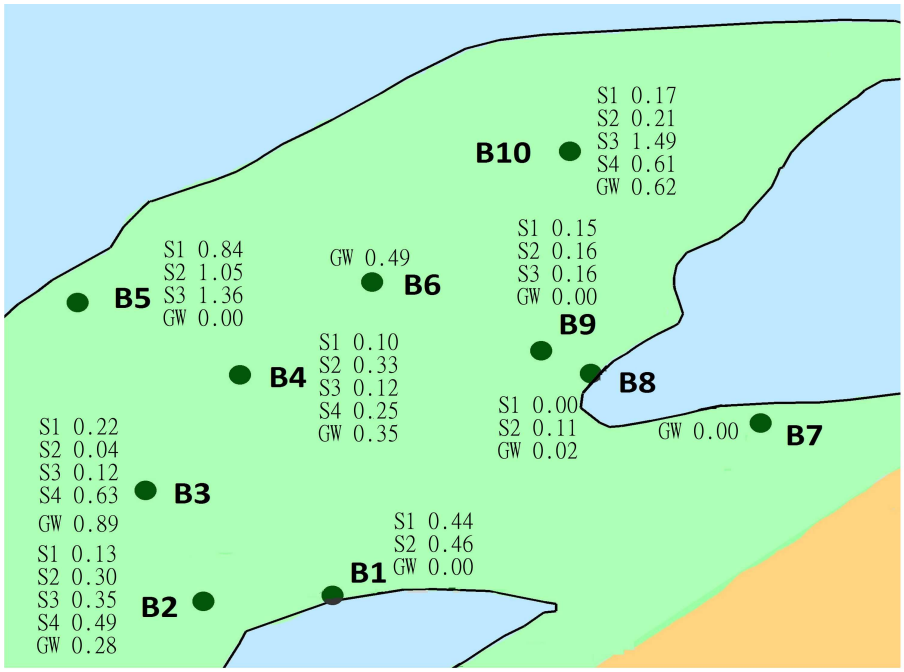

Figure 5.1: The calculated FeS_2 oxidation in mmol/l.

laboratory. However, by combining both IC and ICP-OES data calculated pyrite oxidation between 0.01 mmol/l and 0.21 mmol (T1B1S1) was estimated. Measurements of B1B3 indicate higher excesses of sulphate. These three pore water measurements with chloride concentration around 400 mmol/l plot above the mixing line in figure 5.3a. However, the excess can not be stated with absolute certainty since the chloride measurements were inaccurate.

IJmuiden beach has a few points of interest with respect to high concentrations of excess sulphate. For example, the groundwater of T1B1 has a calculated pyrite oxidation of 0.53 mmol/l at a f_{sw} of 0.03. In addition groundwater of T1B2 and T2B2 have a pyrite oxidation of respectively 0.35 and 0.42 mmol/l at a f_{sw} of 0.34 and 0.11. Detailed results of T1B1 and T1B2 are added in table 5.1. However, the measurements of pore water show lower excess concentrations compared to the groundwater. Also, no pattern of concentration levels with depth could be detected.

Figures 5.2c, 5.4c and 5.3c display the alkalinity for the three sites studied. The alkalinity levels differ significantly from the expected ratio as indicated by the mixing line. Moreover, the largest variation is visible in fresh pore water, where the expected levels are exceeded by 7.75 mmol/l for the Sand Motor and by 8.0 mmol/l and 14.0 mmol/l in Noordwijk and IJmuiden respectively.

Figure 5.5 shows the development of alkalinity and pH with increasing concentrations of excess sulphate in the groundwater of the Sand Motor and IJmuiden. Noordwijk data is not included in this figure, since not enough data is available to indicate a trend. According to formula 2.1 the oxidation of pyrite produces sul-

phate and acid, reducing the pH and alkalinity. However, this process is not shown in figure 5.5, since the graph generally indicates increasing alkalinity levels with higher sulphate concentrations, as well as near-constant pH values. Conversely, concentrations of sulphate and alkalinity in the pore water of IJmuiden and the Sand Motor showed a more random pattern. A depth-dependant pattern of alkalinity, pH and excess of sulphate could not be determined, although, the general trend on the Sand Motor seems to indicate higher alkalinity levels and excess of sulphate in deeper samples at sites with a thick unsaturated zone.

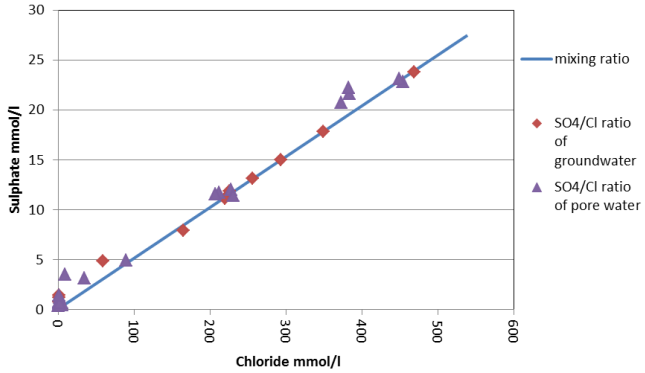

(a) Sulphate in groundwater and pore water over the fresh and salt water range.

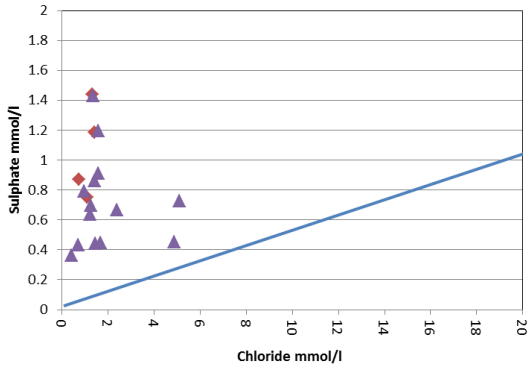

(b) A zoom of figure 5.2a.

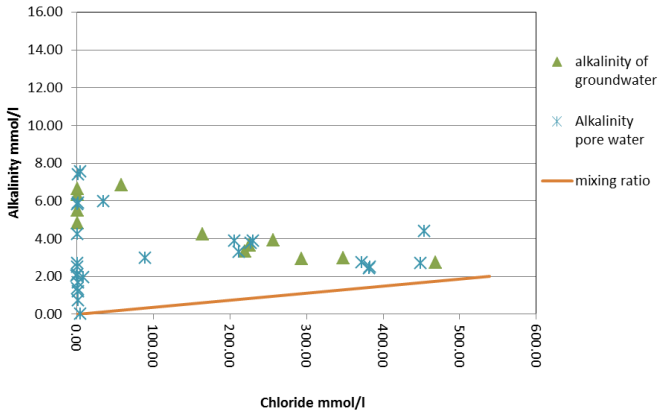

(c) Alkalinity in groundwater and pore water over the fresh and salt water range.

Figure 5.2: The sulphate/chloride and alkalinity/chloride ratio in the groundwater and pore water of the Sand Motor.

Table 5.1: Detailed data of a selection of sampling points from the Sand Motor and IJmuiden which showed interesting results.

Sample	Sampling depth	pH	Alkalinity	Calculated FeS_2 oxidation
units	m	-	mmol/l	mmol/l
Sand Motor				
B2S1	0.88	7.77	1.36	0.13
B2S2	1.78	8.02	2.11	0.30
B2S3	2.77	7.65	1.19	0.35
B2S4	3.58	8.51	7.41	0.49
B2 GW	3.56	9.59	6.31	0.28
B3S1	0.40	8.06	2.70	0.22
B3S2	0.90	8.73	7.57	0.04
B3S3	1.42	8.47	5.90	0.12
B3S4	2.03	8.43	5.99	0.63
B3 GW	2.06	8.09	6.85	0.89
B10S1	0.80	3.37	0.00	0.17
B10S2	1.60	7.23	0.73	0.21
B10S3	2.80	8.05	1.94	1.49
B10S4	3.20	7.88	5.83	0.61
B10 GW	3.35	8.30	6.63	0.62
IJmuiden				
T1B1S1	0.70	8.00	3.19	0.08
T1B1S2	1.25	8.73	13.42	0.09
T1B1S3	1.84	8.61	10.61	0.07
T1B1S4	2.20	8.45	14.02	0.09
T1B1 GW	2.09	8.31	14.19	0.53
T1B2S1	0.20	7.70	5.88	0.48
T1B2S2	0.57	7.56	3.99	0.00
T1B2S3	0.94	7.61	3.35	0.16
T1B2 GW	0.77	7.42	3.15	0.35

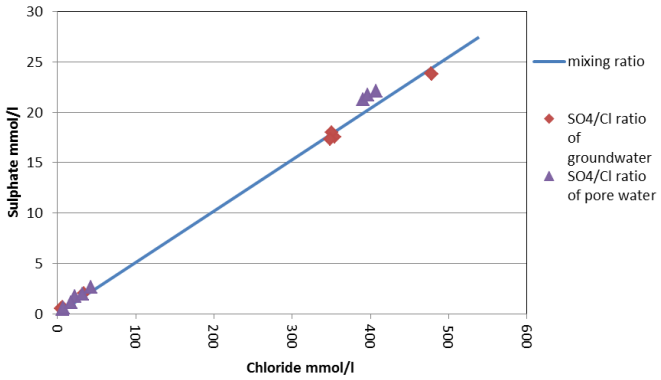

(a) Sulphate in groundwater and pore water over the fresh and salt water range.

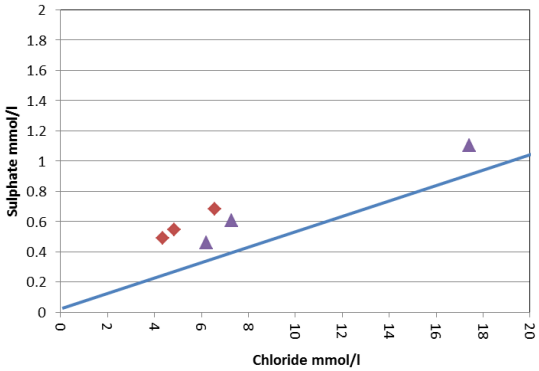

(b) A zoom of figure 5.3a.

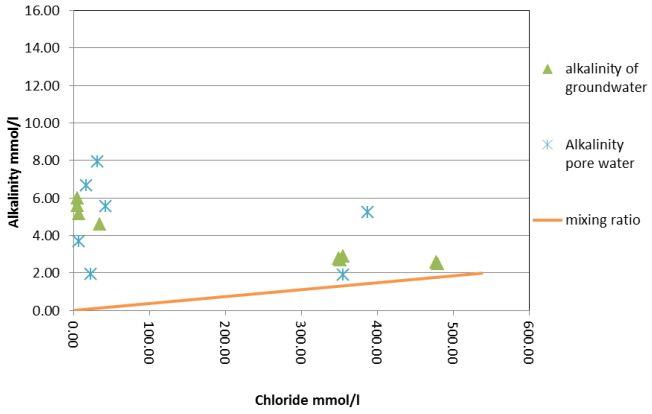

(c) Alkalinity in groundwater and pore water over the fresh and salt range.

Figure 5.3: The sulphate/chloride and alkalinity/chloride ratio in the groundwater and pore water of the beach of Noordwijk. The cluster of three pore water samples above the mixing line with chloride concentrations around 400 mmol/l have a high uncertainty due to underestimation of chloride.

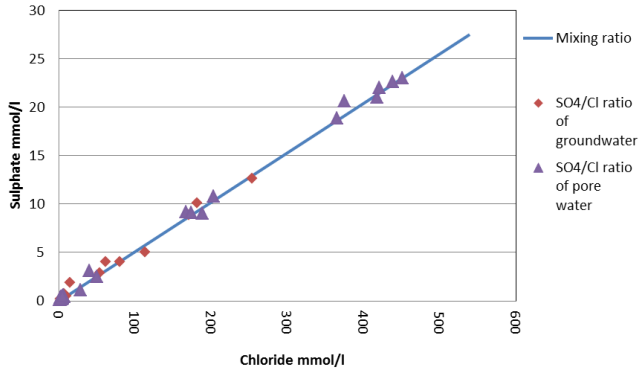

(a) Sulphate in Groundwater and pore water over the fresh and salt water range.

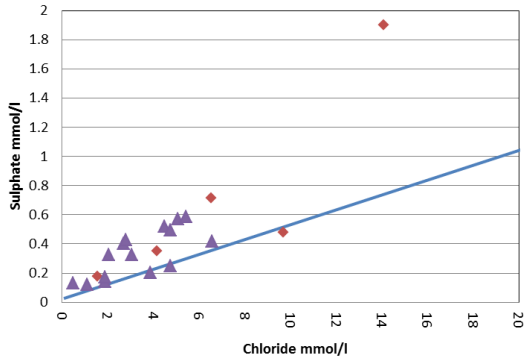

(b) A zoom of figure 5.4a.

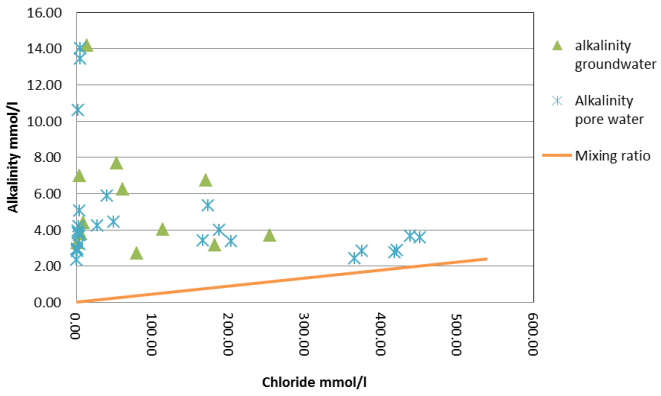

(c) Alkalinity in Groundwater and pore water over a small range of fresh water.

Figure 5.4: The sulphate/chloride and alkalinity/chloride ratio in the groundwater and pore water of IJmuiden beach.

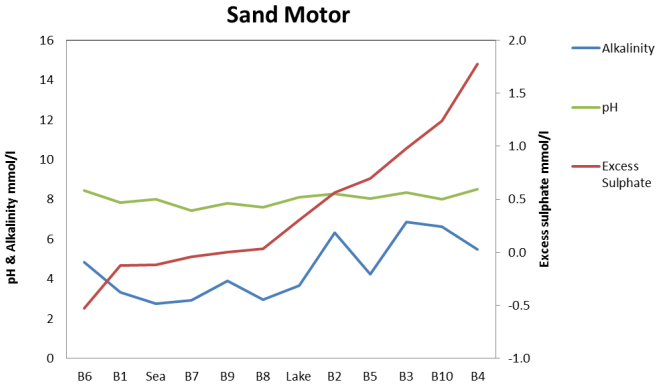

(a) Groundwater of the Sand Motor.

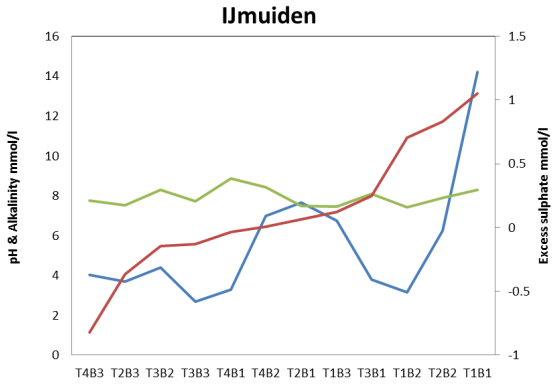

(b) Groundwater samples from IJmuiden.

Figure 5.5: The groundwater data of the Sand Motor and IJmuiden organised with increasing excess sulphate levels.

5.2 Iron concentrations

Another indication of pyrite oxidation is iron oxide. Iron is released from the mineral after pyrite oxidation, after which it precipitates as iron oxide ($Fe(OH)_3$) at circumneutral pH (reaction pathways in figure 2.1). The presence of iron oxide therefore may be indicative for oxidation of pyrite at neutral pH, however, in case of the suppletion, it must be taken into account that iron oxide could also be derived from elsewhere.

In the Sand Motor sand brown iron oxide was observed (figure 5.6). Iron oxide in the sand was seen at B1, B2, B4 and B10 (figure 5.7). At B4 it was noted that brown sand was present directly underneath the surface and at B10 iron oxide was seen at a depth of 3 m.

Figure 5.6: The different Sand Motor sand colors. The brown at the bottom of the core is iron oxide, the grey and brownish sand is the normal sand color. The dark grey sand is organic matter (Pit, 2013).

The iron concentrations in the groundwater of the Sand Motor are too low to measure on the ICP-MS. Only the groundwater of sampling point B10 contains a significant amount of 126 μg/kg iron. In comparison, the highest iron groundwater concentration was measured at B5 in spring 2012, where the groundwater contained 1447 μg/l. Moreover, that year measurements near the slufter contained up to 2880 μg/l.

Concentrations of iron in the pore water are relatively higher compared to the iron concentrations in groundwater, as can be seen in figure 5.7. But a depth-dependant pattern can not be determined. Pore water samples from B2 were taken twice due to an accident during measurement, however the second round of samples taken at approximately the same location shows strongly reduced concentra-

tions of iron. B2S1(1) contains 2564 μg/kg, while B2S1(2) shows $\pm$0 μg/kg. This indicates that the iron content in pore water is locally highly variable.

Comparison between the excess of sulphate, as described in section 5.1, and the iron concentrations renders information on the ratio of soluble iron and iron oxide. In general more than 95% of iron assumed to be derived from pyrite oxidation has precipitated as iron oxide. Exceptions are B2S1 and B3S2, where the precipitated percentage is around 80%.

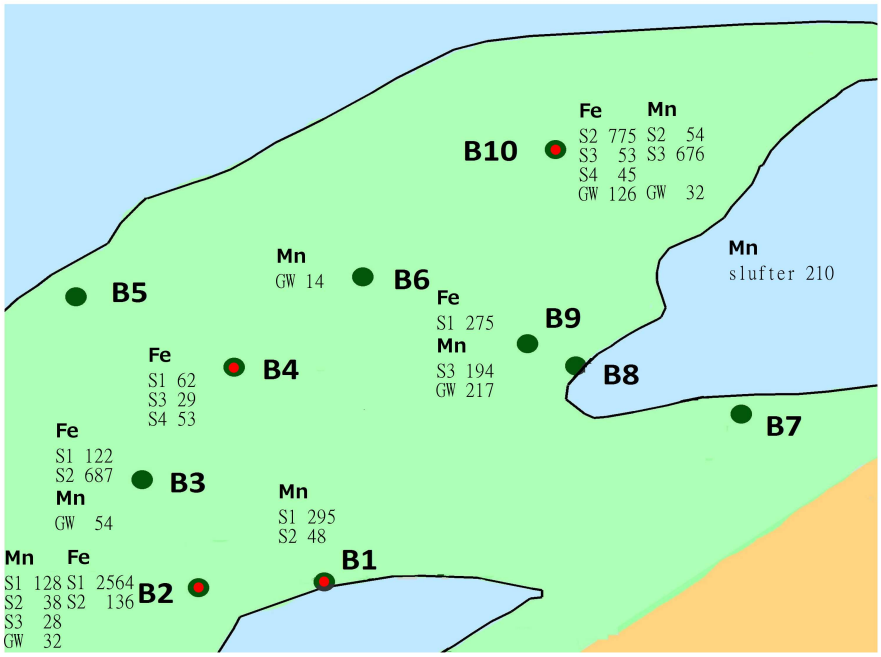

Figure 5.7: The iron and manganese concentrations in the ground- and pore water of the Sand Motor. The concentrations are in μg/kg. The remaining sampling locations and depths contained a concentration too low to measure. The red dots indicate the presence of iron oxide.

In Noordwijk T1B2S1 (0.20 m depth) has a concentration of 107 μg/kg, which, seems to correspond with the iron oxide seen there during fieldwork in the lower lying tidal zone. The ratio soluble Fe/Fe oxide is 82%. Other water samples have a concentration too low to measure. In IJmuiden, iron oxide was observed during drilling at T1B1, T1B4, T2B1, T2B2, T3B2 and T4B1. The groundwater at T4B1 and T4B3 contains respectively 182 and 268 μg/kg of iron and the upper pore water measurements of T1B1 and T1B2 contains 71 and 219 μg/kg of iron. Finally, a high iron concentration of 308 μg/kg is measured at T3B2S3. The ratio soluble Fe/Fe oxide is more than 99%.

Concluding, all locations show high spatial variability in iron concentrations with concentrations ranging from below detection limit to 2564 μg/kg on the Sand

Motor. Additionally, iron oxides and soluble iron seem to occur simultaneously.

5.3 Trace elements

A third result of pyrite oxidation are trace elements. Trace elements can be incorporated in the mineral and in case of presence they are released upon oxidative dissolution of the mineral pyrite. Oxidation can increase their levels in the water unless the elements are re-adsorbed. Thus, elevated concentration of trace elements can indicate pyrite oxidation.

Trace elements are present in both ground- and pore water. Manganese is the only element measured in increased concentrations in the groundwater of the Sand Motor (figure 5.7). The highest groundwater concentration of 217 μg/kg is measured at B9.

Table 5.2 presents trace elements in pore water. Both the amount and element type show a high variability over both space and depth, but in general the concentrations are slightly higher compared to the groundwater. The concentrations for the elements cobalt and cadmium are close to detection limit and will not be considered any further.

The chromium concentration in the pore water of the Sand Motor is in general low, however, a value exceeding the target value for shallow groundwater (Staatscourant, 2012) is measured in B2. Manganese also shows increased concentrations in the pore water of B1, B2, B9 and B10. Nickel is strongly elevated in the top measurements of B2. More importantly, the measurement of 348 μg/kg Ni exceeds the intervention value of 75 μg/kg (Staatscourant, 2012) by far. The concentration of copper is also high at B2S1. Zinc is present in elevated concentrations exceeding the target value for shallow groundwater concentration at the top of B1, B2, B3, B4. The highest Zn concentration in depth can be seen at B2S3, where the value of 1603 μg/kg is double the intervention value.

Concluding, B2 shows the highest concentrations for the different trace elements. However, similar to the iron concentrations (section 5.2), the re-sampling of B2S1 and B2S2 shows highly decreased concentrations of the trace elements.

Finally, the trace element concentrations are plotted against the excess sulphate concentrations to check whether the concentration peaks would appear together. A clear match peak is only seen at B10S3 for the element manganese (figure 5.8).

A few locations were previously measured for trace elements byTuinenburg (2012), therefore, a comparison can be made. The groundwater results are indicated in table 3.3. Additionally, the 2012 results were measured with lower detection limits, therefore, the data gives more detailed information about the lower concentrations.

Arsenic is not measured for the current research, however, the 2012 data indicates that the concentrations exceed the target value for shallow groundwater. Cobalt, copper and nickel were previously measured more accurate. The results indicate that the elements are present in low concentrations in groundwater, whereas

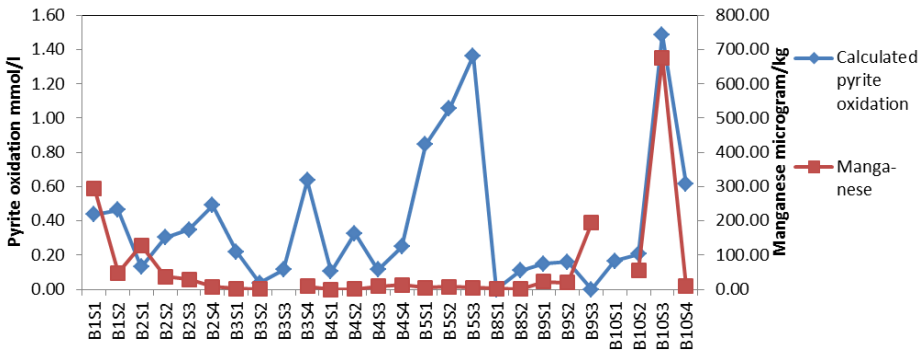

Figure 5.8: The calculated pyrite oxidation and manganese concentrations in the pore water of the Sand Motor. The gaps in the Mn line is missing data. B10S3 shows clearly matching peaks.

the 2013 data indicates significantly higher trace element concentrations in pore water. The chromium concentrations frequently exceed the target value. Finally, iron and manganese concentrations give similar results for 2012 and 2013, however, the locations of concentration peaks in 2012 are not the same as the peaks in 2013.

The trace element concentrations measured in both the groundwater and the pore water of Noordwijk are below detection limit. The single exception is an elevated zinc concentration of 137 μg/kg in the groundwater at T1B3. The samples taken in IJmuiden show higher trace element concentrations (table 5.3). The elements chromium, cobalt, copper, cadmium and lead only occurred at concentrations close to detection limits. The concentrations of zinc, molybdenum and nickel are occasionally higher. Finally, manganese is present in elevated concentrations in a selection of both pore and groundwater.

Table 5.2: The trace elements in the pore water in μg/kg of the Sand Motor. The $\pm$ sign means that the measurements were below detection limit and no accurate concentration can be indicated. Max represents the target value for the element in shallow groundwater (Staatscourant, 2012). The orange values exceed target value, the red numbers are very high or exceed intervention values.

Sample	pH	Cr	Mn	Ni	Cu	Zn	Pb	Mo
Max		1	-	15	15	65	15	5
Detection limits		11.7	14.2	13.3	13.5	12.7	5.9	8.0
ZMB1S1	7.52	±0	295	19.4	±0	50.4	±0	±0
ZMB1S2	7.52	±0	48.0	±0	±0	±0	±0	±0
ZMB2S1	7.77	28.6	128	348	23.3	162	±0	±0
ZMB2S2	8.02	±0	37.8	27.7	±0	95.8	±0	±0
ZMB2S3	7.65	±0	28.4	24.2	±0	1604	±0	±0
ZMB2S4	8.51	±0	±0	±0	±0	±0	±0	±0
ZMB3S1	8.06	±0	±0	±0	±0	177	±0	±0
ZMB3S2	8.73	±0	±0	±0	±0	49.3	±0	±0
ZMB3S4	8.43	±0	±0	±0	±0	±0	±0	±0
ZMB4S1	8.04	±0	±0	±0	±0	194	±0	±0
ZMB4S2	8.22	±0	±0	±0	±0	±0	±0	±0
ZMB4S3	7.98	±0	±0	±0	±0	±0	±0	±0
ZMB4S4	8.30	±0	±0	±0	±0	±0	±0	±0
Detection limits		29.8	28.8	28.7	26.6	28.0	14.1	23.0
ZMB5S1	8.00	±0	±0	±0	±0	±0	±0	±0
ZMB5S2	7.70	±0	±0	±0	±0	±0	±0	±0
ZMB5S3	7.69	±0	±0	±0	±0	±0	±0	±0
ZMB8S1	7.57	±0	±0	±0	±0	±0	±0	±0
ZMB8S2	7.43	±0	±0	±0	±0	±0	±0	±0
ZMB9S1	8.14	±0	±0	±0	±0	±0	±0	±0
ZMB9S2	7.66	±0	±0	±0	±0	±0	±0	±0
ZMB9S3	7.90	±0	194	±0	±0	±0	±0	±0
ZMB10S2	7.23	±0	54.4	48.3	±0	60.5	±0	±0
ZMB10S3	8.05	±0	676	±0	±0	31.0	±0	±0
ZMB10S4	7.88	±0	±0	±0	±0	±0	±0	±0

Table 5.3: The trace elements in the pore and groundwater in μg/kg of the beach of IJmuiden. The $\pm$ sign means that the measurements were below detection limit and no accurate concentration can be indicated. Max represents the target value for shallow groundwater (Staatscourant, 2012).

Sample	pH	Mn	Ni	Zn	Mo
Max		-	15	65	5
Detection limits		14	13	13	8
T3B2 GW	8.28	59.6	$\pm$0	$\pm$0	$\pm$0
T3B3 GW	7.73	734	$\pm$0	$\pm$0	$\pm$0
T4B3 GW	7.77	259	$\pm$0	$\pm$0	$\pm$0
Detection limits		29	29	28	23
T1B1S2	8.73	$\pm$0	$\pm$0	71.5	$\pm$0
T1B1S3	8.61	$\pm$0	$\pm$0	$\pm$0	$\pm$0
T1B2S1	7.70	74.9	66.4	44.6	$\pm$0
T1B4S3	8.03	36.7	$\pm$0	$\pm$0	32.1
T3B3S2	7.83	309	$\pm$0	$\pm$0	$\pm$0

5.4 Freshening of the Sand Motor aquifer

In the Sand Motor an active freshening process is occurring, influencing seawater fractions and the element concentrations in the water. Also the alkalinity levels are affected by this process.

The fraction of seawater (f_{sw}) present in the groundwater of the Sand Motor is indicated in figure 5.9. The originally salt groundwater has been freshened by rainwater, which results in freshwater in the middle of the Sand Motor. The f_{sw} of pore water largely corresponds with the fraction measured in the groundwater. However, the pore water samples of B5 and B8, located close to the water, show higher seawater fractions compared to the groundwater. The slufter and the lake exhibit marine characteristics.

The seawater fractions in Noordwijk are as can be expected, increasing levels of salt water towards the seaside of up to 0.89. The same pattern is visible at the beach of IJmuiden, but there the seawater fractions are much lower. At the northern side the highest f_{sw} fraction is 0.47, while the southern sampling points contains a seawater fraction of 0.21 at a distance of 100 m from the shoreline. This low fraction coincides with seepage from the dunes on the beach. Additionally, the samples were taken on a rainy day, whereas other field days occurred in dryer periods of time.

The main element composition of the groundwater of the Sand Motor is indicated in figure 5.10 by Stiff diagrams. The freshening of the aquifer has advanced the furthest in the middle of the Sand Motor, where the concentrations of sodium, potassium, chloride and magnesium have decreased significantly. The freshening of B2, B4, B6 and B10 is clearly indicated by the high ratios of bicarbonate/chloride. Sodium and chloride are, however, still the dominant components in the water due to the slow change of exchanger occupation of sodium for calcium resulting in a $NaHCO_3$ watertype. In points B2 and B6 freshening has advanced the furthest, since the water is changing towards a $CaHCO_3$-type with equal concentrations of sodium + potassium, calcium and magnesium. This results in the highest calcium/chloride ratio.

The saturation indices (SI) of the water samples have been calculated for gypsum and calcite. The SI of gypsum ($CaSO_4 \cdot 2\,H_2O$) is undersaturated for all samples, which means that the mineral will dissolve rather than precipitate. The results for calcite are different (table 5.4). Locations which are actively freshening (B1, B3, B5, B9) show positive SI values, indicating oversaturation for calcite. The groundwater of B3 is freshening most strongly given the supersaturation for calcite. The already freshened locations of B2, B4 and B10, which should contain a $Ca(HCO_3)_2$-watertype, give, contrary to expectations, undersaturation for calcite, of which B10S2 indicates the strongest undersaturation. The negative values correspond with low alkalinity levels. Additionally, the undersaturation for calcite in B2 and B10 coincides with soluble iron and trace elements. Also, low pH and high calculated pyrite oxidation correspond in the case of B10.

The gradual change from fresh to salt water in Noordwijk and IJmuiden is

shown in figure 5.11. Sodium + potassium, chloride, magnesium and sulphate are the dominant elements in salt water. The stiff diagrams show a strong increase in alkalinity levels in fresh water compared to the calcium, especially in IJmuiden. However, freshening of the groundwater, as is clear on the Sand Motor, is in Noordwijk and IJmuiden not so distinct.

The calcite saturation index is also calculated for Noordwijk en IJmuiden. The SIs for Noordwijk are generally positive, however, a strong undersaturation is calculated for the tidal zone of T1B1 and more moderately for the unsaturated zone of T1B3. The result of T1B1 coincides with lower pH (6.46) and elevated calculated pyrite oxidation (groundwater 0.21 mmol/l). The results of T1B3 correspond with the highly uncertain calculated pyrite oxidation and the presence of zinc. In IJmuiden T1B1 shows the strongest oversaturation, while the pore water of transect 3 and 4 is overall undersaturated. The oversaturation of T1B1 coincides with a high alkalinity, an elevated calculated pyrite oxidation and soluble iron and trace elements. The undersaturation for southern transects mainly corresponds with seepage from the dunes exfiltrating on the beach.

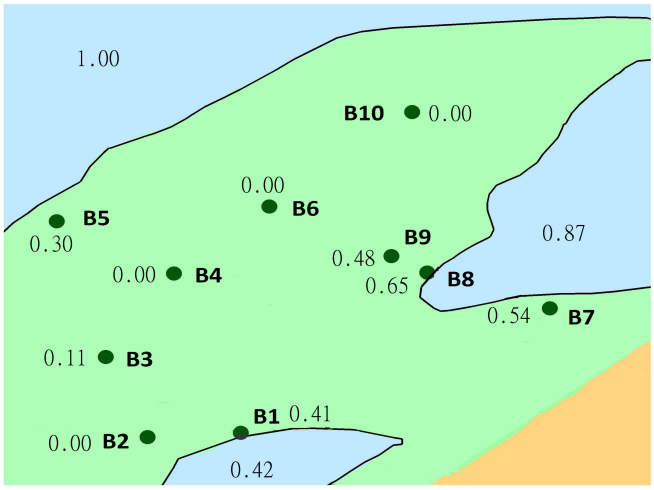

Figure 5.9: The numbers indicate the fraction of seawater present in the groundwater.

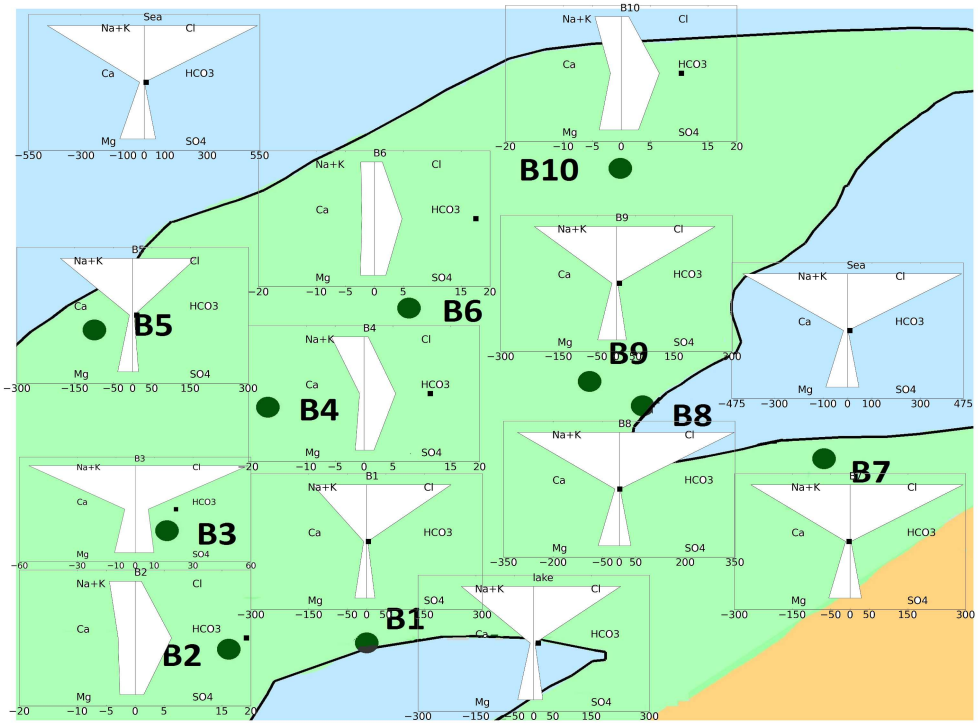

Figure 5.10: Composition of the groundwater on the Sand Motor is indicated with stiff diagrams. The concentrations are in meq/l. The black dot at HCO_3 indicates the calcite saturation index. Beware, the axes change in concentration among the diagrams.

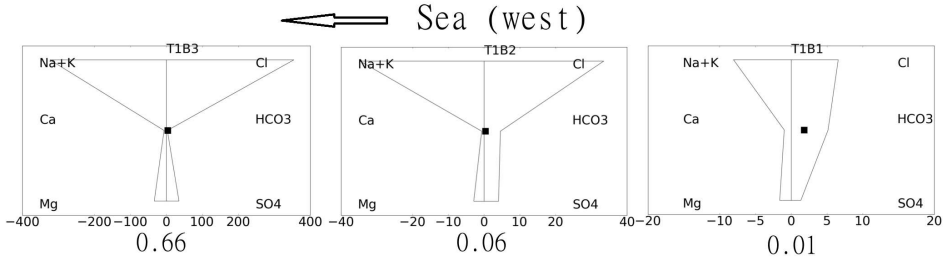

(a) Transcect 1 Noordwijk. The distance towards sea during low tide is approximately 75, 45 and 25 m.

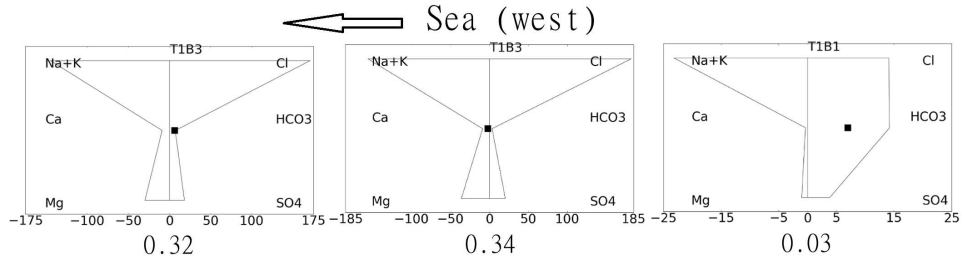

(b) Transcect 1 IJmuiden. The distance towards sea during low tide is approximately 200, 280 and 300 m.

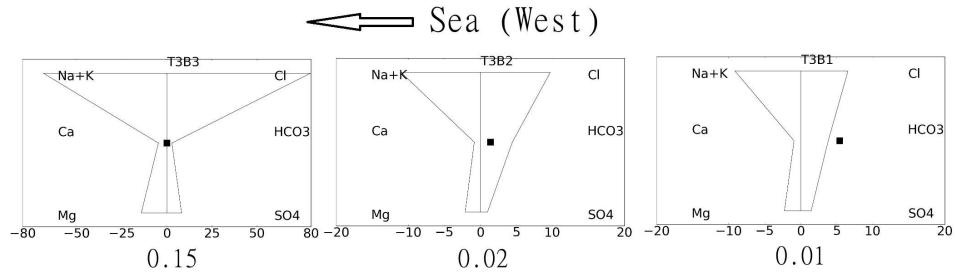

(c) Transcect 3 IJmuiden. The distance towards sea during low tide is approximately 160, 290 and 320 m.

Figure 5.11: Stiff diagrams indicate the gradual change from fresh to salt water for different transects in Noordwijk and IJmuiden. The groundwater composition is in meq/l. The black dot at HCO_3 indicates the calcite saturation index. Beware, the axes change in concentration among the diagrams. The number below represent the seawater fraction.

Table 5.4: The calcite saturation index of the ground- and pore water of the Sand Motor. The red negative numbers are undersaturated with respect to calcite, the positive blue number is supersaturated with respect to calcite.

Sample	pH	Alkalinity	SI calcite
		mmol/l	
B1S1	7.52	3.29	0.02
B1S2	7.52	3.87	0.08
B1 GW	7.83	3.31	0.23
B2S1	7.77	1.36	-0.35
B2S2	8.02	2.11	0.18
B2S3	7.65	1.19	-0.42
B2S4	8.51	7.41	0.85
B2 GW	8.29	6.31	0.96
B3S1	8.06	2.70	0.04
B3S2	8.73	7.57	0.51
B3S4	8.43	5.99	0.88
B3 GW	8.34	6.85	1.06
B4S1	8.04	2.04	-0.03
B4S2	8.22	2.50	0.30
B4S3	7.98	1.67	-0.18
B4S4	8.3	4.24	0.34
B4 GW	8.52	5.49	0.57
B5S1	8.0	2.75	0.43
B5S2	7.7	2.48	0.17
B5S3	7.69	2.42	0.15
B5 GW	8.04	4.24	0.55
B6 GW	8.44	4.83	0.88
B7 GW	7.42	2.93	-0.12
B8S1	7.57	4.39	0.30
B8S2	7.43	2.72	-0.03
B8 GW	7.61	2.96	0.09
B9S1	8.14	2.96	0.21
B9S2	7.66	3.76	0.15
B9S3	7.9	3.90	0.47
B9 GW	7.81	3.91	0.41
B10S2	7.23	0.73	-1.24
B10S3	8.05	1.94	0.37
B10S4	7.88	5.83	0.31
B10 GW	8.02	6.63	0.52
Lake	8.12	3.65	0.60
Slufter	8.02	2.74	0.50

5.5 Comparison of results 2012 and 2013

Figure 5.12 indicates the chemical changes in the Sand Motor over time. B1, B2, B7, B8 and B9 were measured in spring 2012 (Tuinenburg, 2012), summer 2012 (Deltares, 2012) and spring 2013, while B4 and B5 were only measured twice in spring. Additionally, S4T7 and S3T5 were measured twice in 2012, but were added due to interesting results. First, the general trend in seawater fractions is increasing fresh water fractions in the groundwater (figure 5.12a). Second, the pH levels seem relatively stable as can be seen in figure 5.12b. Third, the calculated pyrite oxidation shows a wide variation, of which B2 seems to clearly indicate a trend in the occurrence of oxidation processes in time (figure 5.12c). Finally, figure 5.12d indicates different effect on the alkalinity. The alkalinity of B2 is decreasing, while other measurements show stability or an increase over time.

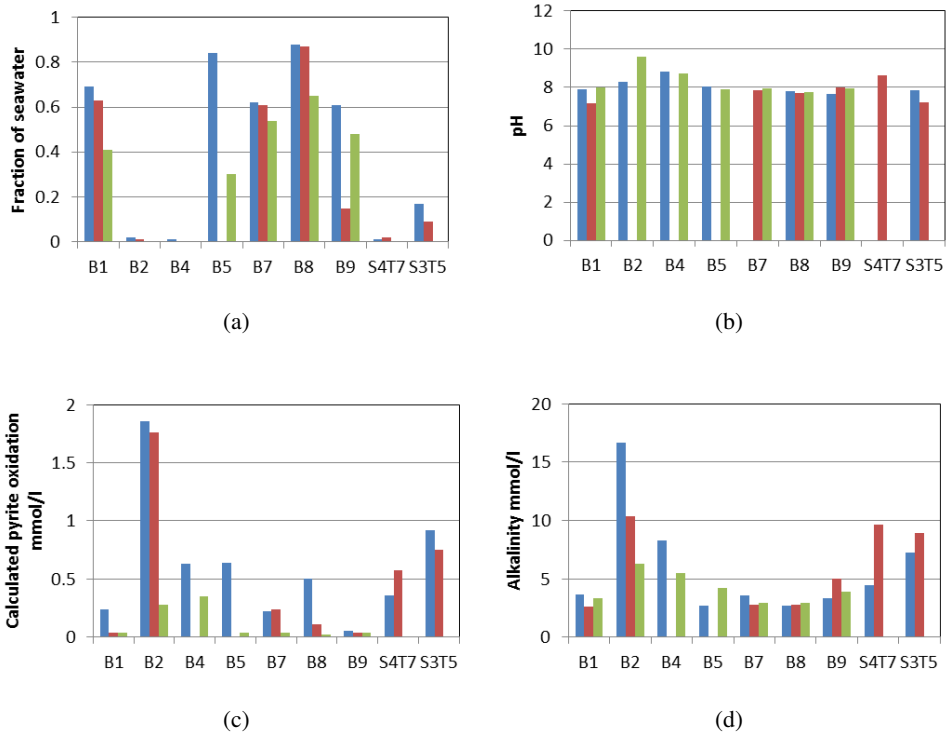

Figure 5.12: Summary of data from corresponding sampling points from 2012 and 2013. Blue is spring 2012 (Tuinenburg, 2012), red is summer 2012 (Deltares, 2012), green is data from the current research. The data gaps indicate missing data.

5.6 CS analysis

Pyrite in sediment can be detected by measurement of sulphur concentrations. A sediment analysis can therefore give an indication of the amount of pyrite present in the sand. Thus, the carbon and sulphur contents of sand samples were determined to get a quantitative indication of pyrite.

Table 5.5 shows the highest carbon content on the beach of IJmuiden and the lowest in Noordwijk, whereas the sulphur content does not differ much among the three locations. The carbonate content of the sediment is assumed to be roughly 4% for the Sand Motor, 3% in Noordwijk and 6% in IJmuiden.

Table 5.5: Summary of CS analyses on pore water sediments in weight percentages.

	Sand Motor	Noordwijk	IJmuiden
Average C_{total}	0.709	0.485	1.028
Average $C_{organic}$	0.299	0.140	0.355
Average S_{total}	0.034	0.030	0.036
Minimum S_{total}	0.027	0.024	0.028
Maximum S_{total}	0.043	0.034	0.052
Average $S_{inorganic}$	0.031	0.029	0.033
Minimum $S_{inorganic}$	0.017	0.022	0.026
Maximum $S_{inorganic}$	0.041	0.033	0.044

5.7 Micro XRF and microprobe

Finally, the presence of pyrite on the Sand Motor was proven by micro XRF and the microprobe. Sand from two sampling locations on the Sand Motor was analysed. The micro XRF analysis indicated grains which could contain pyrite. The grains indicated by the red arrows in figure 5.13 are examples of selected grains.

Analysis of the selected grains by the microprobe proved the presence of pyrite at the locations B3 and B10 at a depth of respectively 2 and 3 meters. A good example of pyrite is shown in figure 5.14, where pyrite is present in its characteristic framboidal shape. Pyrite was observed on larger calcite, feldspar or mica grains, but no independent pyrite grains were observed. Also, iron oxide was measured in the sediment.

The average compositions with standard deviations of 16 pyrite grains are shown in figure 5.15. The identified pyrite grains were often too small to capture the entire beam of the microprobe, therefore, the surroundings of the grains were occasionally included in the measurement. However, better measurements were performed on pyrite cluster formations. Unfortunately, the size of the grains prevented precise measurement, thus occurrence of trace elements in the pyrite could not be determined.

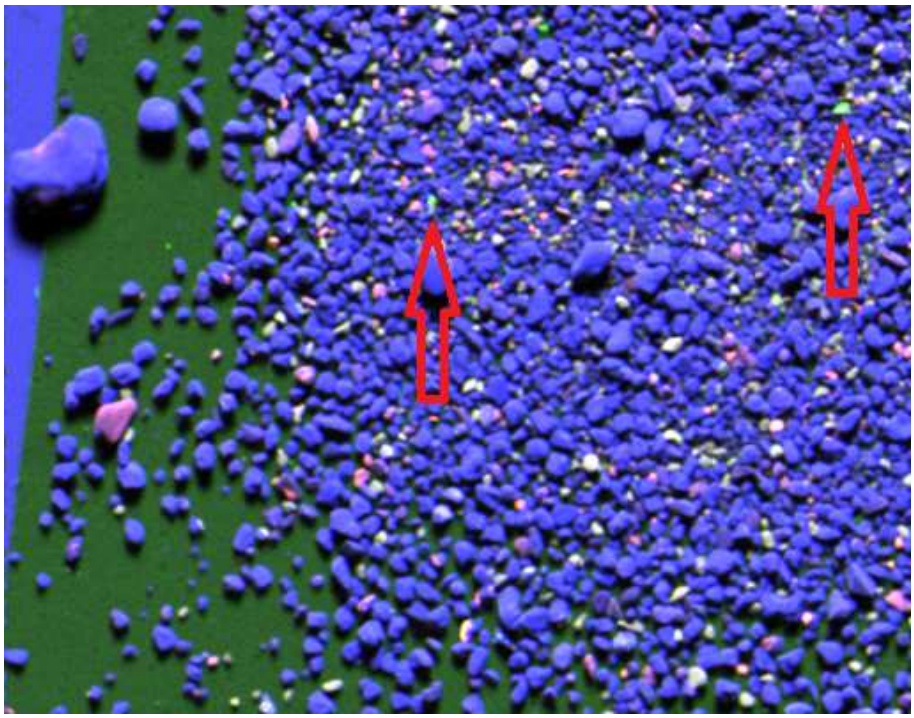

Figure 5.13: The blue, red and green colors indicate the presence of silicate, iron and sulphate respectively. Pyrite is indicated by mixing of green and red resulting in a yellow color. The red arrows point to possible pyrite grains. The grain size varies from 1 mm to 0.1 mm. The pink grains contain both iron and silicate.

In addition, another prominent result of the microprobe analyses was the presence of metal grains with a high concentration of iron, chromium and nickel (figure 5.16). This is the composition of stainless steel, but it can also be iron oxide with included chromium en nickel traces. The grains were present as bright patches on larger grains of calcite, feldspar and pyroxene. This composition was present more often than pyrite. Figure 5.16 consists of the average composition of 7 of these grains. Furthermore, figure 5.17 shows that iron and manganese often occur together as an oxide.

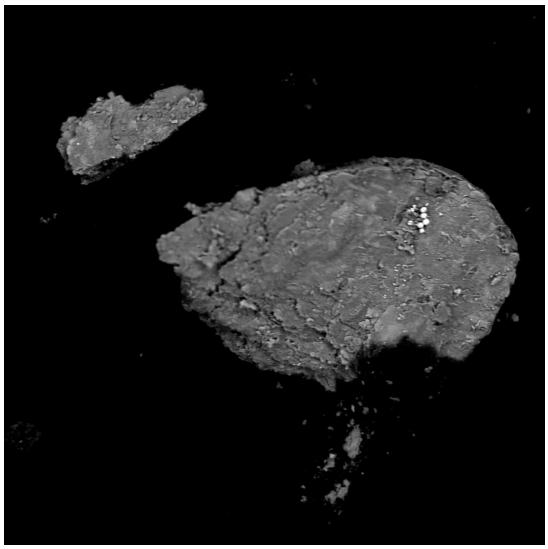

Figure 5.14: A feldspar grain in the B3S4 sample. The small white dots are framboidal pyrite. The framboids are around 5 μm, making the feldspar grain about 0.25 mm long.

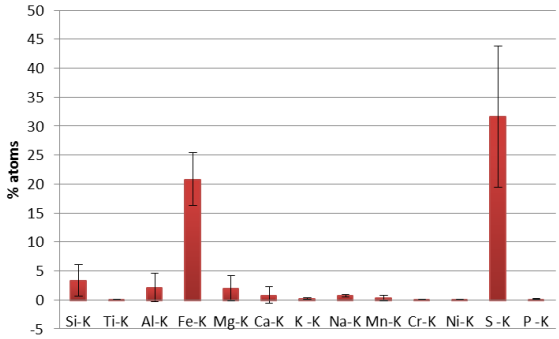

Figure 5.15: Average measurement of 16 pyrite grains on larger calcite, feldspar or mica grains. The ratio of Fe/S approaches 1:2 corresponding with the molar ratio in FeS_2. The measurements of the other elements are mainly caused by accidental inclusion of the matrix during measurement.

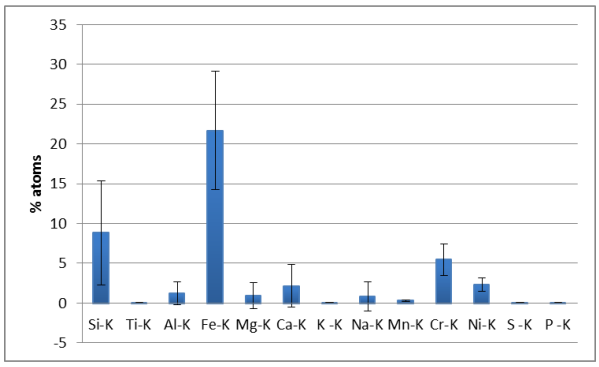

Figure 5.16: The relatively high concentrations of Fe, Ni and Cr in grains attached to larger calcite, feldspar or pyroxene grains. The graph is an average of 7 measurements

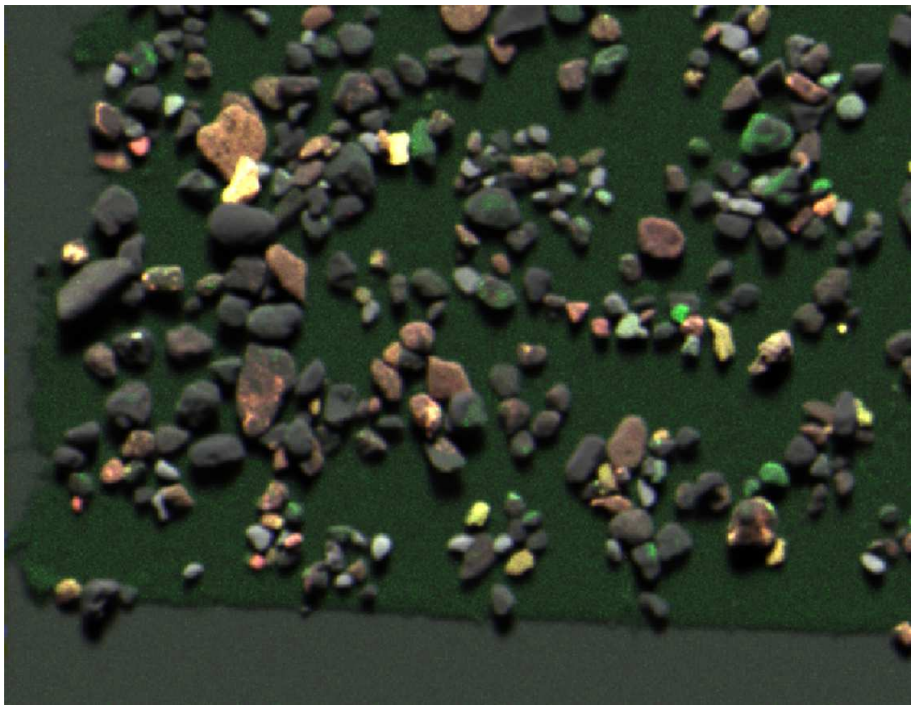

Figure 5.17: Mixing of the elements iron and manganese by the micro XRF, sample derived from B10S4. Oxidised iron and manganese often occur together. Grains with a yellow color indicate both Fe and Mn in the same grain. Red or pink is iron and green is manganese.

Chapter 6

Discussion

This research aims to indicate whether substantial pyrite oxidation is taking place at the Sand Motor compared to the other fieldwork locations. Another question is if pyrite oxidation has an impact on the buffering capacity and to what extent freshening influences these processes. Most importantly, this research would like to indicate if the Sand Motor project could have a negative effect on its environment.

6.1 Freshening

The Sand Motor was a salt aquifer due to the construction with sea sediments. Both ground- and pore water contained high concentrations of sodium, potassium, magnesium and chloride. The ground- and pore water of the Sand Motor have been freshening due to infiltration of rainwater.

The process has advanced the furthest in the middle of the Sand Motor, where the influence of seawater is the lowest. There, the freshening is almost finished, resulting in seawater fractions of 0.00. An exception is B3, where freshening is an active process. This could be caused by finer sediment preventing rapid infiltration of rainwater.

The change to freshwater induces cation exchange, which causes Na^+ initially adsorbed to the exchanger to change for Ca^{2+} stimulating calcite dissolution. Consequently, the additional dissolution of calcite increases the buffer and raises the alkalinity levels. The freshening is proven by the calcite oversaturation in both ground- and pore water. Comparison of 2013 data with 2012 results indicates that freshening has progressed.

No clear freshening processes have been measured in the ground- and pore water of Noordwijk. However, the highest alkalinity level of 14.19 mmol/l is measured in IJmuiden. The groundwater sample was taken in a small dune with marram grass coverage. The high concentration is probably caused by a combination of cation exchange and organic matter, whose presence is confirmed by a high organic carbon content in the sand. Organic matter is consumed by organisms resulting in the release of carbon dioxide in the soil. Dissolution of CO_2 in water

produces carbonic acid (H_2CO_3), but the acid is buffered by calcite in the sand, resulting in an increase of the alkalinity and thereby the pH (Appelo and Postma; Barber, 1995).

Remarkably low seawater fractions are measured close to the coastline further south on the beach of IJmuiden. The low fractions are caused by seepage resulting from infiltration in the western dune area. A wet beach due to seepage was observed on the beach close to the dunes. No freshening occurs here since the sand is in balance with the water content, which results in undersaturation of calcite rather than oversaturation.

6.2 Pyrite oxidation

Microprobing confirms the presence the pyrite for two Sand Motor samples. However, the sulphur measurements on sediments from all three fieldwork locations do not differ much, therefore, large-scale presence of pyrite on the Sand Motor is not proven.

The occurrence of pyrite oxidation on the Sand Motor is indicated by excess of sulphate in both the ground- and pore water and observations of iron oxides. This confirms the hypothesis of pyrite oxidation occurring on the Sand Motor. The calculated pyrite oxidation in Noordwijk is more moderate. IJmuiden shows, contrary to expectations, higher levels of calculated pyrite oxidation in mainly the groundwater.

The excess of sulphate at the Sand Motor does not show a spatial trend, but samples from larger depth indicate a higher extent of pyrite oxidation. However, higher sulphate concentrations in the tidal zone or saturated zone may be derived from pyrite oxidation occurring in the unsaturated zone, since sulphate is mobile in the dominantly pH neutral sands (Appelo and Postma).

Comparison with 2012 data shows a general decrease of calculated pyrite oxidation in groundwater. This might indicate a decrease of pyrite oxidation intensity, while previous excess sulphate concentrations have been flushed.

Larsen and Postma (1997) measured the groundwater composition in the unsaturated zone of an aquifer where pyrite oxidation occurred as a consequence of lowering of the groundwater depth. Concentrations of sulphate excess correspond to the concentrations measured in pore water of the Sand Motor, which are occasionally even higher.

The acid produced by pyrite oxidation has not caused an overall low pH or strongly reduced buffering capacity at the Sand Motor. Calcareous sands buffers the acidification. Additionally, the freshening process increases the alkalinity further. The high alkalinity levels can in general be found in samples taken at larger depth, which corresponds to the higher excess of sulphate. However, a few exceptions were observed. Highly acid pore water with corresponding zero alkalinity and a strong undersaturation of calcite is measured at the northern side of the Sand Motor (B10). Additionally, these results coincide with a high calculated pyrite oxi-

dation. Further south on the Sand Motor (B2) the calculated pyrite levels are much lower, but comparison with 2012 data shows previously high calculated pyrite oxidation and a strong decrease of alkalinity levels over the year. Although no acid conditions are measured here, pyrite oxidation has a clear impact on the buffering capacity of the sand. Concluding, even though the measurements indicate overall neutral pH and intact buffer capacities, data does suggest that the buffer capacity is negatively influenced by pyrite oxidation.

A striking trend is the highly elevated concentrations of alkalinity in mainly the fresh water range for all three locations. This can be explained by freshening combined with the depth of the unsaturated zone. Fresh water occurs in the middle of the Sand Motor or higher up on the beach towards the dunes. These are the highest locations of the beach. The height results in a deep unsaturated zone where pyrite oxidation can take place. High alkalinity levels were not expected in Noordwijk, since freshening is not an active process and the estimated pyrite oxidation is moderate. Possibly, the high buffer capacity is a remainder of former pyrite oxidation or freshening.

6.3 Iron and manganese

Oxidation of pyrite releases Fe^{2+}, which readily oxidises and precipitates as Fe^{3+} oxides. The oxidation decreases the soluble amounts of iron in the water, which, normally, has a minimum solubility in pH range 7.5 to 8.5 in calcareous soils (Lindsay, 1991). No soluble iron was expected in the ground- and pore water due to the overall neutral-pH measurements.

However, contrary to expectations, both 2012 and 2013 data suggests significant amounts of soluble iron in groundwater en pore water. Larsen and Postma (1997) also observed soluble iron in pH neutral waters. This was explained by depletion of oxidisers (O_2 and nitrate) by pyrite oxidation, after which, not enough electron acceptors are available to oxidise iron. Therefore, soluble iron indicates an incomplete oxidation process.

However, the pore water data indicates high levels of soluble iron in the unsaturated zone where an abundance of oxygen is available. In general more than 95% and occasionally around 80% of the iron derived from pyrite oxidation precipitates. The presence of the remaining soluble iron can either be caused by slow precipitation processes, or, it indicates that pyrite oxidation is an active process. However, the high iron concentrations near the surface in B10 and B2 coincide with low pH and decreasing alkalinity levels, respectively. Therefore, these soluble iron concentrations might be caused by acidification at the top of the unsaturated zone, which prevents precipitation of iron.

High iron concentrations were measured in the sulfter in 2012. This could be caused by a different mechanism than mentioned earlier. In the slufter organic matter settles due to the low flow velocity, as was observed by Pit (2013) (figure 6.1). The organic matter can form soluble complexes with iron. In reduced en-

Figure 6.1: Organic matter in the slufter, as observed by Pit (2013).

vironments complexes between iron and natural organic matter (NOM) can form which are relatively stable and strong. Additionally, besides Fe, also Mn, Zn and Cu can be adsorbed on these complexes (Barber, 1995), explaining the corresponding high concentration of manganese in the groundwater. The complexes regulate the bioavailability of metal ions by making them more soluble (Rose and Waite, 2003), thus increasing the cation concentration in solution (Barber, 1995). Therefore, the complexation process of iron with local NOM can cause accumulation of the element resulting in high groundwater concentrations.

The element manganese is present in high concentrations in the pore water and occasionally the groundwater of the Sand Motor. Similar to iron, manganese can be present in pyrite, incorporated as main trace element (Roskam and Griffioen, 2011). Also, oxidation of manganese sulphide (MnS), which is much more soluble than pyrite, can cause high concentrations. Both Fe and Mn can precipitate as oxide, separately or together in oxidized environments (Larsen and Postma, 1997; Appelo and Postma).

Since iron and manganese behave similarly, high levels of manganese in reduced environment can thus be caused by a lack of oxidisers, whereas in the unsaturated zone the concentrations are a consequence of slow precipitation or active oxidation processes. Furthermore, the iron concentrations of B10 and B2 have corresponding soluble manganese concentrations. Concluding, high concentrations of both iron and manganese in pore water can be caused by mobilisation in local acidic conditions of the unsaturated zone.

In Noordwijk the presence of iron is less prominent, however, the single significant concentration measured in pore water of the unsaturated zone corresponds

to moderate levels of calculated pyrite. Slightly higher concentrations of both iron and manganese were measured at IJmuiden beach, which coincide with elevated levels of calculated pyrite oxidation. Since no indications of low pH or depletion of oxygen were found for both locations, the soluble iron might be an indication of locally active pyrite oxidation.

6.4 Trace elements

Calcite buffering was predicted to prevent mobilisation of the cation trace elements, which were expected to be incorporated in the pyrite. Elevated concentrations of oxyanion trace elements were anticipated, assuming their presence in pyrite.

The oxyanion trace elements are in general not present in significant amounts (arsenic is not measured). This could mean that either the elements are not incorporated in pyrite or the conditions are not favourable for solution. However, the dominantly pH-neutral pore water contains occasionally significant amounts of cation trace elements in both the unsaturated zone and the tidal zone. A few samples show a strong accumulation for zinc and nickel, which exceed both target values and intervention values for shallow groundwater. The highest concentrations of trace elements are present in the earlier mentioned B10 and B2, which coincide with low pH and decreasing alkalinity levels.

The elevated concentrations of nickel and zinc in comparison with copper, lead and cadmium are higher, because the latter elements are more strongly sorbed to iron oxides compared to nickel and zinc in the dominantly near-neutral pH (Appelo and Postma).

The accumulation leading to peak concentrations can be caused by a pyrite oxidation front in the unsaturated zone. Kjoller et al. (2004) demonstrated that an acidification front in the soil forms a geochemical trap for trace elements. Downward moving acidic ground- or pore water containing trace elements passes the acidification front, below which trace elements are adsorbed to manganese and iron oxides due to the increase in pH. Henceforth, the elements are again desorbed when the front advances. In time this process results in accumulation of trace elements at the acidification front.

Acidified pore water has only been measured at B10. However, locations in the middle of the Sand Motor have an unsaturated zone of more than two meters deep. As a consequence, the first pore water samples were taken at a depth between 0.4 to 0.9 m deep. Hence, it might be possible that acid conditions occur higher up in the unsaturated zone, which was not sampled. Additionally, Larsen and Postma (1997) showed a significant elevation of nickel and manganese in the unsaturated zone at a pH of 6.75, therefore, a strong decrease in pH conditions would not even be necessary to increase the trace element concentrations. Still, it must be noted that the pH, alkalinity and trace element accumulation do not fully correspond.

Roskam and Griffioen (2011) measured the trace element content in pyrite minerals in clay sediments, resulting in trace element/pyrite ratios. The ratio is 4.3 mg

of manganese per gram pyrite, 0.32 mg Pb/g, 0.28 mg As/g, 0.11 mg Co/g, 0.09 mg Ni/g and 0.08 mg Zn/g. First, the groundwater trace element data of Tuinenburg (2012), which was measured with lower detection limits, is compared. Manganese corresponds with the ratio resulting in the most dominant trace element. The order of magnitude also fits for cobalt and nickel. The arsenic ratio slightly overestimated the amount of arsenic. The ratio for zinc is significantly to low, the measured groundwater levels are one order higher. Second, the current ground- and pore water results are compared with the ratios. Again the manganese corresponds well. Arsenic data is not available and the detection limits could not measure cobalt or lead accurate enough. However, the measured zinc and nickel concentrations are up to 2 orders of magnitude larger than the ratios estimated. Concluding, the majority of trace elements corresponds to the ratios, therefore, the assumption is made that the trace elements are derived from pyrite. The underestimation of nickel and zinc can be due to higher amounts of pyrite-incorporated zinc and nickel at the Sand Motor or additional zinc and nickel is derived from other sources.

The major trace elements in the water of the Sand Motor are iron and manganese. Therefore, it is not likely that the metal oxides as showed in figure 5.16 are the source of the iron concentrations in the groundwater, since the trace element ratios of chromium and nickel do not correspond.

The trace elements in Noordwijk are negligible compared to the Sand Motor. The trace element/pyrite ratios indicated elevated manganese concentrations, however, this was not measured. The other trace element estimations are below detection limit. The IJmuiden beach shows a few elevated nickel, zinc and molybdenum concentrations, which coincide with elevated sulphate excess. The concentrations besides manganese do not correspond with trace element estimations. This can either be due to the detection limits, the lack of pyrite or incorporated trace elements. Also, limited mobilisation is possible as a result of neutral pH. The few peak concentrations exceed the estimated amounts, which might indicate additional sources of trace elements.

Interesting differences between sample locations of the Sand Motor are visible when comparing all parameters assumed to be related with pyrite oxidation. An example is the occurrence of high concentrations of trace elements without corresponding sulphate levels. The missing sulphate is presumed to have dispersed by infiltrating rain, since sulphate is mobile and not adsorbed in the dominantly pH neutral sands (Appelo and Postma). This process can also explain the sharp decrease of iron concentrations between 2012 and 2013. The movement of trace elements is retarded due to secondary adsorption at circum neutral pH to iron and manganese oxides (Stipp et al., 2002; Larsen and Postma, 1997). A second example is the measurement of pyrite oxidation without corresponding elevated trace elements. These locations are still buffered by calcite dissolution reducing the solubility of the elements.

The differences between the two examples demonstrate that the process of pyrite oxidation can be at different stages. Locations where trace elements but no sulphate is found indicate ceasing oxidation processes since no new sulphate is

produced. Locations were elevated sulphate but no trace elements have been found are at an earlier stage, when the buffer still remains and possibly more pyrite is present to oxidise.

6.5 Method

With all things considered, a few things must be kept in mind when using the research data. The selected sampling locations and samples cover only a small part of the total study sites. The results do therefore give a representative indication of the reality. Additionally, less data is available for Noordwijk, which increases the uncertainty of conclusions.

Furthermore, the limitations of the measured trace element data as described in chapter 4 must be noted. The high detection limits prevented accurate measurements. Additionally, groundwater measurements from 2012 (table 3.3) seem to show much higher trace element concentrations, since the detection limits in 2012 were much lower. Moreover, it is important to note that the sampling of pore water of IJmuiden transect 1 after centrifuging was done without additional precautions preventing pollution of the samples, as were added for later sampling.

Also, when comparing data between 2012 and 2013 it should be taken into account that the GPS locations in 2012 were saved with a hand GPS, which at best has an accuracy of 3 m. This inaccuracy is also partially applicable for the remeasurement for pore water, since the very exact DGPS (accuracy around 1 cm) broke down during the pore water fieldwork campaign. Therefore, the comparability of the results from the 'same' location can be questioned.

6.6 Sand Motor assessment

The goal of the large-scale suppletion site the Sand Motor is the protection of the local coastline for the coming 20 years, thereby preventing repeated disruption of the environment. Large-scale suppletion can become more common if the Sand Motor pilot proves to be save and effective in all its aspects. The aim of this research is to indicate whether pyrite oxidation in combination with aquifer freshening might be a hazard for the Sand Motor in comparison to traditional suppletion and a control site. Current data and comparison with 2012 data indicate a few points of interest. Pyrite oxidation processes are taking place or have been taking place mainly in the middle of the Sand Motor where freshening has also advanced the furthest. The processes have lead to increased concentrations of sulphate and iron in the water. These elevated concentrations are higher on the Sand Motor compared to the traditional suppletion and control site. However, chemical consequences in general have remained limited due to the large buffering capacity of the calcareous sands. The locations where the buffering capacity has been (partially) depleted gives a clear insight in the chemical consequences. There, the pyrite trace

elements accumulated in the pore water, resulting in exceeding of target values for shallow groundwater and occasionally in crossing of the intervention values.

Concluding, although long-term monitoring should show if these elevated concentrations are temporal or will persist for longer periods of time, this research indicates that trace elements should remain a subject of interest.

6.6.1 Traditional suppletion

The research data shows moderate signs of active pyrite oxidation on the traditional suppletion site, the beach of Noordwijk. Even though the beach received significant suppletion volumes in 2008, the possible effects of pyrite oxidation in the freshly oxidised sand may have already disappeared for the largest part. Both sulphate and possible trace elements can have dispersed. The high alkalinity present might be a remnant of former pyrite oxidation or cation exchange followed by calcite dissolution.

6.6.2 Control site

The control site IJmuiden did show some interesting results. Trace element data indicated a few locations with elevated concentrations. At first sight an explanation could be influence of precipitated emissions of the factories of Tata Steel located north of the sampling sites in IJmuiden. However, the results coincide with an excess of sulphate, iron oxide and soluble iron, which for a few cases is comparable to results measured at the Sand Motor. The results would induce a conclusion of pyrite oxidation, however, the sand of IJmuiden has not been artificially disturbed in the last decade. Also, the washing ashore of pyrite minerals derived from suppletion sites elsewhere seems unlikely. Therefore, pyrite oxidation is not expected to be the cause. Concluding, IJmuiden is a location requiring further research to gain insight in the mechanisms and causes behind the elevated concentrations of sulphate, iron, and trace elements. It would be interesting to see if micro XRF and microprobing could identify pyrite grains there.

Chapter 7

Conclusions and recommendations

7.1 Conclusions

This research confirms that pyrite oxidation occurs on the Sand Motor. However, comparison of sulphur content of sand from the three field locations does not demonstrate large-scale presence of pyrite on the Sand Motor. Nonetheless, the effects are most prominent in the unsaturated zone in the middle of the Sand Motor where freshening has advanced the furthest. The tidal zone did not significantly differ in pyrite oxidation from the unsaturated zone or the saturated zone. The buffering capacity is generally high as suggested by the overall neutral pH conditions and alkalinity levels. Additionally, freshening of the aquifer increases the alkalinity in the groundwater by carbonate dissolution induced by cation exchange during freshening. Still, acidification is expected to occur at the top of the unsaturated zone due to the mobile iron and trace element concentrations in the pore water. An acidification front can have caused accumulation of trace elements exceeding both shallow groundwater target values and occasionally intervention values.

The traditional suppletion site shows moderate signs of (former) pyrite oxidation. However, contrary to expectation, data from the control site does suggest pyrite oxidation. Further research on the control site would thus be interesting.

7.2 Recommendations

Finally, a few recommendations for further research. This research is the third small-scale fieldstudy of the Sand Motor. In order to construct a thorough timeline, it would be interesting to keep remeasuring the sampling locations. A selection of locations can be made to study in detail based on the results. Current data suggests that pyrite oxidation is most prominent in the top of the unsaturated zone. Therefore, sampling there would be recommended. Furthermore, it is recommended

to model the measured iron, sulphate, pH and alkalinity levels with the chemical program PHREEQC.

Additionally, the IJmuiden data showed a few unexpected results. Microprobing could prove whether pyrite minerals are present there. Finally, a tip, experience shows that performing fieldwork on a Dutch beach in spring or summer is much more agreeable compared to winter.

Chapter 8

Acknowledgements

I would like to thank professor Jasper Griffioen from Utrecht University for supervising my master thesis project. I also want to thank MSc. Iris Pit for helping me with advise, preparing and performing fieldwork and exploring the laboratory. The introduction in the subject by Rob Tuinenberg was very constructive. Finally, Deltares and especially Mike van der Werf have been very helpful with lending fieldwork equipment, a car and twice even the four-wheel drive.

Bibliography

Akcil, A. and Koldas, S. (2006). Acid Mine Drainage (AMD): causes, treatment and case studies. *Journal of Cleaner Production*, 14(12-13 SPEC. ISS.):1139–1145.

Alley, R. B., Hewitson, B., Hoskins, B., Joos, F., Jouzel, J., Kattsov, V., Lohmann, U., Manning, M., Matsuno, T., Molina, M., et al. (2007). Summary for policymakers.

Andersen, M. S., Larsen, F., and Postma, D. (2001). Pyrite oxidation in unsaturated aquifer sediments. reaction stoichiometry and rate of oxidation. *Environmental science & technology*, 35(20):4074–4079.

Appelo, C. A. J. and Postma, D. *Geochemistry, groundwater and pollution*. A.A. Balkema Publishers.

Bakker, M., Van Heteren, S., Vonhgen, L., Van Der Spek, A., and Van Der Valk, B. (2012). Recent coastal dune development: Effects of sand nourishments. *Journal of Coastal Research*, 28(3):587–601.

Barber, S. A. (1995). *Soil nutrient bioavailability: a mechanistic approach*. Wiley.com.

Berner, R. A. (1984). Sedimentary pyrite formation: an update. *Geochimica et Cosmochimica Acta*, 48(4):605–615.

Bierens de Haan, S. (1991). A review of the rate of pyrite oxidation in aqueous systems at low temperature. *Earth Science Reviews*, 31(1):1–10.

Billon, G., Ouddane, B., Laureyns, J., and Boughriet, A. (2001). Chemistry of metal sulfides in anoxic sediments. *Physical Chemistry Chemical Physics*, 3(17):3586–3592.

Clemente, R., Almela, C., and Bernal, M. (2006). A remediation strategy based on active phytoremediation followed by natural attenuation in a soil contaminated by pyrite waste. *Environmental Pollution*, 143(3):397–406.

Cotter-Howells, J., Campbell, L., Valsami-Jones, E., Batchelder, M., et al. (2000). *Environmental mineralogy, microbial interactions, anthropogenic influences, contaminated land and waste management*. Mineralogical Society.

De Vriend, H. and Van Koningsveld, M. (2012). Building with nature, thinking, acting and interacting differently. Technical report, Ecoshape.

Deltacommissie (2008). Samen werken met water, een land dat leeft, bouwt aan zijn toekomst. Technical report, Deltacommissie 2008.

Deltares (2012). Personal communication J. Griffioen, February 2013.

Dorronsoro, C., Martin, F., Ortiz, I., Garca, I., Simn, M., Fernndez, E., Aguilar, J., and Fernndez, J. (2002). Migration of trace elements from pyrite tailings in carbonate soils. *Journal of Environmental Quality*, 31(3):829–835.

Eijkelkamp (2013). Soil coring with coring tubes and sample ring. Technical report.

Elbaz-Poulichet, F., Dupuy, C., Cruzado, A., Velasquez, Z., Achterberg, E., and Braungardt, C. (2000). Influence of sorption processes by iron oxides and algae fixation on arsenic and phosphate cycle in an acidic estuary (tinto river, spain). *Water Research*, 34(12):3222–3230.

Evangelou, V. and Zhang, Y. (1995). A review: Pyrite oxidation mechanisms and acid mine drainage prevention. *Critical Reviews in Environmental Science and Technology*, 25(2).

Holzhauer, H., Van der Valk, B., Van Dalfsen, J., Baptist, M., and Janssen, G. (2009). Ecologisch gericht suppleren, nu en in de toekomst, het ontwerp meerjarenplan voor monitoring en (toepassingsgericht) onderzoek. Technical report, Deltares.

Huerta-Diaz, M. and Morse, J. (1990). A quantitative method for determination of trace metal concentrations in sedimentary pyrite. *Marine Chemistry*, 29(C):119–144.

Kjoller, C., Postma, D., and Larsen, F. (2004). Groundwater acidification and the mobilization of trace metals in a sandy aquifer. *Environmental Science and Technology*, 38(10):2829–2835.

Landschap Noord-Holland (2013). Personal communication J. Diemeer, February 2013.

Larsen, F. and Postma, D. (1997). Nickel mobilization in a groundwater well field: Release by pyrite oxidation and desorption from manganese oxides. *Environmental Science and Technology*, 31(9):2589–2595.

Lindsay, W. L. (1991). Iron oxide solubilization by organic matter and its effect on iron availability. In *Iron Nutrition and Interactions in Plants*, pages 29–36. Springer.

Mulder, J., Hommes, S., and Horstman, E. (2011). Implementation of coastal erosion management in the Netherlands. *Ocean and Coastal Management*, 54(12):888–897.

Mulder, J. and Tonnon, P. (2010). Sand Engine: Background and design of a mega-nourishment pilot in the Netherlands.

Natura2000 (2013). Kennemerland-zuid. April 2013, `www.synbiosys.alterra.nl/natura2000`.

Oude Essink, G., Van Baaren, E., and De Louw, P. (2010). Effects of climate change on coastal groundwater systems: A modeling study in the Netherlands. *Water Resources Research*, 46(10).

Pit, I. (2013). Photos fieldwork september 2013. Personal communication I. Pit, Utrecht University, Oktober 2013.

Province of Zuid-Holland (2013). Sand Motor. October 2013 `sandmotor.nl`.

Rijkswaterstaat (2012a). Kustonderhoud. December 2012, `www.terstaat.nl/water/veiligheid/bescherming_tegen_het_water/veiligheidsmaatregelen/kustlijnzorg/`.

Rijkswaterstaat (2012b). Toelichting suppletieprogramma 2012-2015. Technical report, Rijkswaterstaat, Minsterie van Infrastructuur en Milieu.

Rijkswaterstaat (2012c). Zandmotor: pilot-project voor natuurlijke kustbescherming. December2012, `www.rijkswaterstaat.nl/water/veiligheid/bescherming_tegen_het_water/veiligheidsmaatregelen/zandmotor/`.

Rimstidt, J. and Vaughan, D. (2003). Pyrite oxidation: A state-of-the-art assessment of the reaction mechanism. *Geochimica et Cosmochimica Acta*, 67(5):873–880.

Rodrigues, S., Henriques, B., Coimbra, J., Ferreira da Silva, E., Pereira, M., and Duarte, A. (2010). Water-soluble fraction of mercury, arsenic and other potentially toxic elements in highly contaminated sediments and soils. *Chemosphere*, 78(11):1301–1312.

Rose, A. L. and Waite, T. D. (2003). Kinetics of iron complexation by dissolved natural organic matter in coastal waters. *Marine chemistry*, 84(1):85–103.

Roskam, G. and Griffioen, J. (2011). Een verkennende studie naar sporenelementen in pyriet in nederlandse geologische afzettingen. Technical report, TNO.

Ruessink, B., van der Grinten, R., Vonhögen-Peeters, L., Ramaekers, G., and Lodder, Q. (2012). Nearshore evolution at Noordwijk (NL) in response to nourishments, as inferred from Argus video imagery. pages 179–183.

Scholz, F. and Neumann, T. (2007). Trace element diagenesis in pyrite-rich sediments of the Achterwasser lagoon, SW Baltic Sea. *Marine Chemistry*, 107(4):516–532.

Schoonen, M. (2004). Mechanisms of sedimentary pyrite formation. *Special Paper of the Geological Society of America*, 379:117–134.

Smedley, P. and Kinniburgh, D. (2002). A review of the source, behaviour and distribution of arsenic in natural waters. *Applied Geochemistry*, 17(5):517–568.

Sohlenius, G. and Born, I. (2004). Geochemistry and partitioning of trace metals in acid sulphate soils in Sweden and Finland before and after sulphide oxidation. *Geoderma*, 122(2-4 SPEC. IIS.):167–175.

Staatscourant (2012). Circulaire bodemsanering 2009. *Staatscourant*, 6563.

Stipp, S., Hansen, M., Kristensen, R., Hochella, M., Bennedsen, L., Dideriksen, K., Balic-Zunic, T., Leonard, D., and Mathieu, H. (2002). Behaviour of Fe-oxides relevant to contaminant uptake in the environment. *Chemical Geology*, 190(1):321–337.

Stolk, A. (2001). Landelijk meetnet regenwatersamenstelling, meetresultaten 2000. Technical report, RIVM.

Stowa (2013). Effect zandsuppletie op kust en waddenzee. July 2013, `deltaproof.stowa.nl/Publicaties/deltafact/Effect_zandsuppletie_op_kust_en_Waddenzee`.

Stronkhorst, J., De Ronde, J., Mulder, J., Huisman, B., Van Aalst, M., Sprengers, C., Van der Valk, B., and Loffler, M. (2011). Onderzoek Alternatieve Lange Termijn Suppletiestrategien (ALS). Technical report, Deltares.

Stuyfzand, P., Arens, S., and Oost, A. (2010). Geochemische effecten van zandsuppleties langs Hollands kust. Technical report, KWR.

Technology Foundation STW (2011). Nature-driven nourishment of coastal systems, NatureCoast. Program Proposal Nature Coast, Perspectief 2011.

Tuinenburg, R. (2012). Locating a fresh water lens and studying pyrite oxidation in the sand engine. Research project of the study Sustainable Developement at Utrecht University.

Van der Sluis, M. Effecten van suppleties op duinontwikkeling. Technical report, Rijkswaterstaat - Waterdienst.

Van Wirdum, G. (1991). *Vegetation and Hydrology of Floating Rich-fens*. Datawyse.

Wang, Q. and Morse, J. (1996). Pyrite formation under conditions approximating those in anoxic sediments: I. pathway and morphology. *Marine Chemistry*, 52(2):99–121.

Appendix A

(a) Sand motor during construction. Photo taken between 18 and 28 June 2011

(b) Photo taken on 13 October 2011

Figure A.1: The development of the Sand motor over time (Province of Zuid-Holland, 2013).

(a) Photo taken on 31 October 2012

(b) Photo taken on 1 October 2013

Figure A.2: The development of the Sand motor over time (Province of Zuid-Holland, 2013).

Figure A.3: The sampled beach of Noordwijk aan Zee.

(a) The broad beach of IJmuiden

(b) Small dune development on IJmuiden beach

Figure A.4

Appendix B

Alkalinity is usually defined as the acid neutralizing capacity of a solution. In seawater alkalinity can be simplified to equation B.1.

$$\text{Alkalinity} = HCO_3^- + 2CO_3^{2-} + OH^- - H^+ \tag{B.1}$$

Introduction

The alkalinity is an operational defined parameter. Usually it is defined as the acid neutralizing capacity of a solution when the end point of the titration is the CO_2 equivalence point. In seawater alkalinity can be simplified as

$$Alk = (HCO_3^-) + 2*(CO_3^{2-}) + (B(OH)^{4-}) + (OH^-) - (H^+)$$

In freshwater alkalinity is usually dominated by bicarbonate and carbonate.

$$Alk = (HCO_3^-) + 2*(CO_3^{2-}) + (OH^-) - (H^+)$$

In practice often an endpoint titration is performed (pH 4.3). A more accurate method is the Gran method, which to linearizes the titration curve close to the equivalence points. Please refer to Stumm&Morgan, Aquatic Chemistry p179 – 186 for a comprehensive description of the method.

Gran Method

To determine the total alkalinity we have to titrate the sample solution with HCl until a pH-value of lower than 4. The pH-values are measured after each addition by a pH-electrode. By plotting the data we will get titrationcurves from which we receive the values of alkalinity of each sample by using the GRAN – METHOD.

The equivalence point is the point where the slope of the tangent at the curve is maximal (≡turning point).

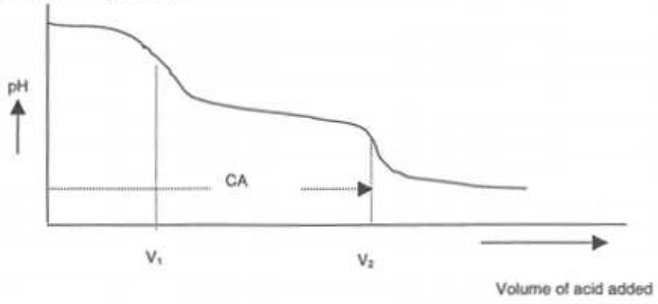

Fig 1: Titration curve of $H_2CO_{3\,(aq)}$

Calculation

The Gran function F1 can be determined by:

$$F1 = (V_0 + V) * 10^{-pH}$$

V_0 = Volume sample
V = Volume acid added

Figure B.1

By plotting the Gran Functions of each meassured point, we receive a graph similar to Fig.2.

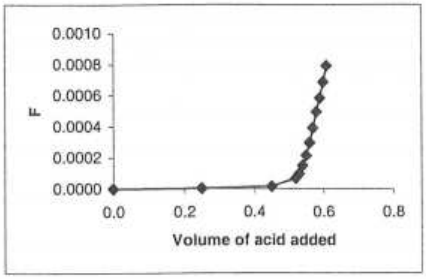

Fig 2: Gran plot for the determination of CA.

We have to interpolate the linear part of the function. The point at axis x where axis y = 0 corresponds to the value of V2 with which we can now calculate the alkalinity.

$$\text{Alkalinity} = (V_2 * C_{HCl}) / \text{Volume}_{Sample}$$

Analysis

Pipette ca. 15 ml in a beaker, add a stirrer and place a pH-electrode in the solution. Add HCl (0.01 M) in (small) steps and write down the resulting pH-values until you reached a pH of about 3.5 (about 15 steps). Create a titration curve and a Gran-function from the received data and estimate the value for the alkalinity.

Sample name	Data point number	Acid added (ml)	pH	Vo + V	10 to the power -pH	F
xxxxx	1	0.000	7.51	2.00	3.09E-08	6.18E-08
Sample vol (ml)	2	0.250	5.96	2.25	1.10E-06	2.47E-06
	3	0.450	5.24	2.45	5.75E-06	1.41E-05
	4	0.520	4.58	2.52	2.63E-05	6.63E-05
2	5	0.530	4.43	2.53	3.72E-05	9.40E-05
Regression points chosen	6	0.540	4.24	2.54	5.75E-05	1.46E-04
	7	0.550	4.08	2.55	8.32E-05	2.12E-04
	8	0.560	3.94	2.56	1.15E-04	2.94E-04
7 to 13	9	0.570	3.82	2.57	1.51E-04	3.89E-04
V2 value (ml) (x = y-c/m)	10	0.580	3.72	2.58	1.91E-04	4.92E-04
	11	0.590	3.65	2.59	2.24E-04	5.80E-04
	12	0.600	3.58	2.60	2.63E-04	6.84E-04
0.531	13	0.610	3.52	2.61	3.02E-04	7.88E-04
Alkalinity (mM)						
2.656						

Figure B.2

Appendix C

Table C.1: The sampling coordinates of the Sand Motor, Noordwijk and IJmuiden.

Sample	X coordinate	Y coordinate
Sand Motor		
B1	451954.88	72514.91
B2	451945.83	72377.66
B3	452163.42	72297.10
B4	452392.47	72421.72
B5	452503.58	72284.97
B6	452598.68	72594.94
B7	452283.77	72981.30
B8	452387.15	72800.70
B9	452431.42	72748.17
B10	452796.45	72817.01
Lake	451960.07	72537.39
Slufter	452315.10	72898.68
Noordwijk		
T1B1	475002.79	90388.40
T1B2	475017.54	90363.77
T1B3	475029.34	90343.76
T2B1	474783.63	90265.28
T2B2	474806.06	90236.43
T2B3	474817.77	90216.34
T3B1	474672.44	90206.75
T3B2	474693.78	90171.58
T3B3	474708.47	90150.31
IJmuiden		
T1B1	497257.41	98430.39
T1B2	497247.18	98415.54
T1B3	497226.65	98342.21
T1B4	497190.49	98246.10
T2B1	497386.30	98429.39
T2B2	497345.00	98319.50
T2B3	497326.91	98263.96
T3B1	495690.04	98918.94
T3B2	495683.72	98887.96
T3B3	495667.41	98759.98
T3B4	495656.06	98660.86
T4B1	495253.42	98840.61
T4B2	495253.65	98825.81
T4B3	495240.75	98711.79

Table C.2: pH, Alkalinity and IC data of the ground- and pore water of the Sand Motor. n.a. means that the element could not be measured. The data accuracy can deviate up to 5%.

Sample	pH	Alkalinity	Fluoride	Chloride	Bromide	Nitrate	sulphate
GW		mmol/l	mg/l	mg/l	mg/l	mg/l	mg/l
B1	7.98	3.31	0.8	7770	26.2	34.5	1070
B2	9.59	6.31	1.3	38	0.2	5.2	72
B3	8.09	6.85	0.9	2076	6.5	0.0	469
B4	8.71	5.49	0.9	26	0.1	0.2	84
B5	7.91	4.24	0.4	5827	19.7	2.2	764
B6	8.15	4.83	0.7	50	0.2	1.7	114
B7	7.94	2.93	0.5	10400	35.2	3.6	1440
B8	7.77	2.96	0.6	12350	41.9	0.0	1715
B9	7.97	3.91	0.5	9084	30.2	0.0	1263
B10	8.25	6.63	0.8	47	n.a.	0.0	138
Lake	8.44	3.65	0.6	7998	26.5	0.0	1142
Slufter	8.28	2.74	1.0	16616	57.3	0.9	2287
PW							
B1S1	7.52	3.29	0.6	7493	26.7	2.4	1127
B1S2	7.52	3.87	0.6	7318	26.0	1.2	1108
B2S1	7.77	1.36	0.7	25	n.a.	8.4	41
B2S2	8.02	2.11	1.0	34	n.a.	10.2	76
B2S3	7.65	1.19	0.9	55	n.a.	10.7	87
B2S4	8.51	7.41	1.5	56	n.a.	1.0	115
B3S1	8.06	2.70	0.2	44	n.a.	8.3	61
B3S2	8.73	7.57	0.9	172	n.a.	8.3	44
B3S3	8.47	5.90	0.7	52	n.a.	8.8	42
B3S4	8.43	5.99	1.5	1235	4.2	n.a.	305
B5S1	8.00	2.75	0.2	15	n.a.	9.8	35
B5S2	7.70	2.48	0.6	50	n.a.	14.9	83
B5S3	7.69	2.42	0.5	59	n.a.	11.6	43
B4S1	8.04	2.04	1.0	44	n.a.	4.1	67
B4S2	8.22	2.50	0.7	13191	47.3	3.9	1989
B4S3	7.98	1.67	0.5	13567	48.6	3.3	2082
B4S4	8.30	4.24	0.5	13532	49.9	3.2	2136
B8S1	7.57	4.39	0.9	16074	54.9	3.7	2194
B8S2	7.43	2.72	1.5	15921	54.2	5.6	2224
B9S1	8.14	2.96	0.3	3170	10.6	20.3	478
B9S2	7.66	3.76	0.5	8077	26.8	0.9	1155
B9S3	7.90	3.90	0.6	8165	27.0	3.5	1097
B10S1	3.37	-0.25	n.a.	181	n.a.	15.3	70
B10S2	7.23	0.73	0.5	84	n.a.	9.8	64
B10S3	8.05	1.94	0.8	300	n.a.	11.3	340
B10S4	7.88	5.83	0.8	47	n.a.	1.6	137

Table C.3: pH, Alkalinity and IC data of the ground- and pore water of Noordwijk. n.a. means that the element could not be measured. The IC pore water data is incomplete. The data accuracy can deviate up to 5%.

Sample	pH	Alkalinity	Fluoride	Chloride	Bromide	Nitrate	sulphate
GW		mmol/l	mg/l	mg/l	mg/l	mg/l	mg/l
T1B1	8.18	5.16	0.3	233	0.7	16.0	65
T1B2	8.46	4.59	1.4	1187	4.1	11.6	195
T1B3	7.75	2.88	0.8	12560	42.8	8.2	1687
T2B1	8.02	6.00	0.3	155	0.5	9.9	47
T2B2	7.77	2.69	0.8	12435	42.7	5.2	1732
T2B3	7.68	2.55	1.0	16928	57.2	4.2	2288
T3B1	8.04	5.57	0.4	172	n.a.	16.8	53
T3B2	7.82	2.78	0.8	12359	42.1	6.4	1659
T3B3	7.76	2.47	1.0	16978	57.2	4.2	2283
PW							
B1S1	8.05	1.93	0.3	796	2.7	43.6	163
B1S2	8.09	2.86	-	-	-	-	-
B1S3	6.46	3.66	0.2	216	n.a.	9.1	54
B1S4	7.56	7.95	1.0	1090	3.6	13.6	168
B2S1	8.62	6.66	1.2	568	2.1	32.9	91
B2S2	8.44	5.54	-	-	-	-	-
B2S3	8.14	5.21	0.4	13734	50.4	7.3	2231
B3S1	7.47	1.89	0.9	12593	45.2	8.1	1958
B3S2	7.47	2.57	-	-	-	-	-
B4S3	7.56	2.63	-	-	-	-	-

Table C.4: pH, Alkalinity and IC data of the ground- and pore water of IJmuiden. n.a. means that the element could not be measured. The data accuracy can deviate up to 5%.

Sample	pH	Alkalinity	Fluoride	Chloride	Bromide	Nitrate	sulphate
GW		mmol/l	mg/l	mg/l	mg/l	mg/l	mg/l
T1B1	8.46	14.19	1.7	499	2.0	18.6	183
T1B2	7.85	3.15	n.a.	6441	22.9	3.9	967
T1B3	7.57	6.75	n.a.	6039	20.2	0.0	855
T2B1	7.58	7.67	0.5	1900	6.6	51.0	280
T2B2	8.05	6.24	0.8	2170	7.1	35.0	391
T2B3	7.69	3.71	n.a.	8998	30.9	11.9	1216
T3B1	8.21	3.79	0.6	231	0.8	44.8	68
T3B2	8.27	4.41	0.7	343	1.2	0.3	46
T3B3	7.80	2.69	0.5	2825	9.4	0.0	389
T4B1	8.79	3.30	0.4	55	0.2	12.2	17
T4B2	8.68	6.97	1.9	147	0.5	10.9	34
T4B3	7.73	4.02	0.7	4019	13.0	0.0	487
PW							
T1B1S1	8.00	3.19	0.5	159	0.5	25.9	50
T1B1S2	8.73	13.42	2.6	180	0.5	14.0	55
T1B1S3	8.61	10.61	1.9	95	n.a.	8.4	39
T1B1S4	8.45	14.02	2.6	192	0.7	7.7	56
T1B2S1	7.70	5.88	1.1	1423	4.7	25.1	301
T1B2S2	7.56	3.99	0.5	6655	21.9	6.8	868
T1B2S3	7.61	3.35	0.8	7198	23.6	5.0	1034
T1B3S1	-	-	1.0	233	0.4	19.1	40
T1B3S2	7.64	3.40	1.3	5909	19.7	2.4	883
T1B3S3	7.58	5.32	1.1	6146	20.6	0.4	877
T1B4S1	7.61	2.75	1.3	14820	49.3	8.7	2018
T1B4S2	7.64	2.42	n.a.	12948	43.2	2.4	1812
T1B4S3	8.03	2.82	1.6	13293	44.6	n.a.	1977
T3B1S1	8.23	4.17	0.7	108	0.3	19.6	31
T3B1S2	7.21	3.83	0.2	99	0.3	21.5	41
T3B1S3	7.95	3.95	0.8	72	0.2	16.8	31
T3B2S1	7.91	2.83	0.1	67	0.2	4.1	13
T3B2S2	7.82	3.84	0.5	136	0.5	1.1	19
T3B2S3	8.50	5.06	1.7	168	0.6	0.8	24
T3B3S1	7.06	4.24	0.4	994	3.2	5.3	111
T3B3S2	7.83	4.43	0.7	1745	6.1	0.9	242
T3B4S1	7.47	2.88	1.4	14920	50.6	5.3	2114
T3B4S2	7.43	3.59	1.3	15978	54.0	10.3	2206
T3B4S3	7.51	3.67	1.0	15539	52.6	8.1	2175
T4B1S1	7.96	2.35	0.2	17	0.1	10.0	12
T4B1S2	7.57	2.96	0.5	39	0.1	8.1	12
T4B1S3	7.84	2.92	0.5	67	0.2	11.2	17
T4B1S4	7.91	3.69	0.6	168	0.5	20.2	47

Table C.5: Trace element data of the ground- and pore water of Sand Motor. ±0 means that the concentration was below detection limit.

Sample	Li	Be	Al	Sc	V	Cr	Mn	Fe	Co	Ni
GW	μg/kg	μg/kg	μg/kg	μg/kg	μg/kg	μg/kg	μg/kg	μg/kg	μg/kg	μg/kg
B1	20.1	±0	±0	±0	±0	±0	±0	±0	±0	±0
B2	±0	±0	±0	±0	±0	±0	31.5	±0	±0	±0
B3	±0	±	±0	±0	±0	±0	54.3	±0	±0	±0
B4	±0	±0	±0	±0	±0	±0	±0	±0	±0	±0
B5	57.0	±0	±0	±0	18.1	±0	±0	±0	±0	±0
B6	±0	±0	±0	±0	±0	±0	14.2	±0	±0	±0
B7	47.5	±0	18.3	±0	21.4	±0	±0	±0	±0	±0
B8	60.5	±0	±0	±0	24.6	±0	±0	±0	±0	±0
B9	34.2	±0	±0	±0	13.0	±0	217.2	±0	±0	±0
B10	±0	±0	±0	±0	±0	±0	32.3	125.6	±0	±0
Lake	33.2	±0	±0	±0	±0	±0	±0	±0	±0	±0
Slufter	79.1	±0	±0	±0	24.4	±0	210.3	±0	±0	±0
PW										
B1S1	48.1	±0	20.8	±0	21.1	±0	295.1	±0	±0	19.4
B1S2	43.2	±0	±0	±0	17.7	±0	48.0	±0	±0	±0
B2S1	±0	±0	231.8	±0	±0	28.6	128.3	2564.2	±0	348.0
B2S2	±0	±0	29.5	±0	±0	±0	37.8	135.8	±0	27.7
B2S3	±0	±0	69.7	±0	±0	±0	28.4	±0	±0	24.2
B2S4	±0	±0	±0	±0	±0	±0	±0	±0	±0	±0
B3S1	±0	±0	64.1	±0	±0	±0	±0	121.5	±0	±0
B3S2	±0	±0	320.1	±0	±0	±0	±0	687.0	±0	±0
B3S4	12.6	±0	17.9	±0	±0	±0	±0	±0	±0	±0
B4S1	±0	±0	45.2	±0	±0	±0	±0	61.8	±0	±0
B4S2	±0	±0	±0	±0	±0	±0	±0	±0	±0	±0
B4S3	±0	±0	62.0	±0	±0	±0	±0	±0	±0	±0
B4S4	±0	±0	55.9	±0	±0	±0	±0	±0	±0	±0
B5S1	107.3	±0	34.6	±0	31.3	±0	±0	±0	±0	±0
B5S2	119.1	±0	±0	±0	24.8	±0	±0	±0	±0	±0
B5S3	113.3	±0	32.4	±0	33.0	±0	±0	±0	±0	±0
B8S1	118.4	±0	±0	±0	34.6	±0	±0	±0	±0	±0
B8S2	107.9	±0	±0	±0	35.7	±0	±0	±0	±0	±0
B9S1	34.3	±0	120.8	±0	13.4	±0	±0	275.3	±0	±0
B9S2	58.4	±0	±0	±0	16.6	±0	±0	±0	±0	±0
B9S3	51.2	±0	±0	±0	20.2	±0	194.5	±0	±0	±0
B10S2	±0	±0	282.4	±0	±0	±0	54.4	775.3	±0	48.3
B10S3	±0	±0	±0	±0	±0	±0	676.3	±0	±0	±0
B10S4	±0	±0	±0	±0	±0	±0	±0	±0	±0	±0

Table C.6: Trace element data of the ground- and pore water of Sand Motor. ±0 means that the concentration was below detection limit.

Sample	Cu	Zn	Sr	Y	Zr	Mo	Cd	Ba	Pb	U
GW	μg/kg	μg/kg	μg/kg	μg/kg	μg/kg	μg/kg	μg/kg	μg/kg	μg/kg	μg/kg
B1	±0	±0	1831	±0	±0	±0	±0	17.4	±0	17.4
B2	±0	±0	713	±0	±0	±0	±0	±0	±0	17.6
B3	±0	±0	1015	±0	±0	±0	±0	±0	±0	42.0
B4	±0	±0	181	±0	±0	±0	±0	±0	±0	15.5
B5	±0	±0	2590	±0	±0	±0	±0	±0	±0	27.8
B6	±0	±0	352	±0	±0	±0	±0	±0	±0	16.8
B7	±0	±0	3247	±0	±0	±0	±0	±0	±0	16.8
B8	±0	±0	3826	±0	±0	±0	±0	±0	±0	16.1
B9	±0	±0	2842	±0	±0	±0	±0	26.8	±0	18.3
B10	±0	±0	486	±0	±0	±0	±0	±0	±0	15.9
Lake	±0	±0	2368	±0	±0	±0	±0	11.0	±0	15.9
Slufter	±0	±0	4822	±0	±0	±0	±0	6.2	±0	14.9
PW										
B1S1	±0	50.4	2932	±0	±0	±0	±0	40.3	±0	20.3
B1S2	±0	±0	2729	±0	±0	±0	±0	25.3	±0	19.8
B2S1	23.3	161.7	268	±0	±0	±0	±0	37.4	±0	17.6
B2S2	±0	95.8	314	±0	±0	±0	±0	±0	±0	20.4
B2S3	±0	1603.8	335	±0	±0	±0	±0	±0	±0	20.3
B2S4	±0	±0	243	±0	±0	±0	±0	±0	±0	43.0
B3S1	±0	177.3	137	±0	±0	±0	±0	±0	±0	20.3
B3S2	±0	49.3	26	±0	±0	±0	±0	±0	±0	25.8
B3S4	±0	±0	549	±0	±0	±0	±0	±0	±0	45.2
B4S1	±0	194.2	210	±0	±0	±0	±0	±0	±0	20.5
B4S2	±0	±0	263	±0	±0	±0	±0	±0	±0	21.8
B4S3	±0	±0	190	±0	±0	±0	±0	21.3	±0	21.3
B4S4	±0	±0	204	±0	±0	±0	±0	±0	±0	23.3
B5S1	±0	±0	3988	±0	±0	±0	±0	±0	±0	±0
B5S2	±0	±0	4167	±0	±0	±0	±0	±0	±0	±0
B5S3	±0	±0	4186	±0	±0	±0	±0	18.8	±0	±0
B8S1	±0	±0	4362	±0	±0	±0	±0	20.8	±0	±0
B8S2	±0	±0	4429	±0	±0	±0	±0	23.6	±0	±0
B9S1	±0	±0	510	±0	±0	±0	±0	±0	±0	±0
B9S2	±0	±0	2189	±0	±0	±0	±0	24.7	±0	±0
B9S3	±0	±0	2391	±0	±0	±0	±0	32.6	±0	±0
B10S2	±0	60.5	175	±0	±0	±0	±0	±0	±0	±0
B10S3	±0	31.0	736	±0	±0	±0	±0	±0	±0	±0
B10S4	±0	±0	451	±0	±0	±0	±0	±0	±0	±0

Table C.7: Trace element data of the ground- and pore water of Noordwijk. ±0 means that the concentration was below detection limit. The data is incomplete.

Sample	Li	Be	Al	Sc	V	Cr	Mn	Fe	Co	Ni
GW	μg/kg	μg/kg	μg/kg	μg/kg	μg/kg	μg/kg	μg/kg	μg/kg	μg/kg	μg/kg
T1B1	±0	±0	±0	±0	±0	±0	±0	±0	±0	±0
T1B2	±0	±0	±0	±0	±0	±0	±0	±0	±0	±0
T1B3	72.0	±0	±0	±0	23.8	±0	±0	±0	±0	±0
T2B1	±0	±0	±0	±0	±0	±0	±0	±0	±0	±0
T2B2	66.9	±0	±0	±0	24.2	±0	±0	±0	±0	±0
T2B3	84.6	±0	±0	±0	34.0	±0	±0	±0	±0	±0
T3B1	±0	±0	±0	±0	±0	±0	±0	±0	±0	±0
T3B2	64.4	±0	±0	±0	22.3	±0	±0	±0	±0	±0
T3B3	80.3	±0	±0	±0	35.5	±0	±0	±0	±0	±0
PW										
T1B1S3	±0	±0	±0	±0	±0	±0	±0	±0	±0	±0
T1B1S4	±0	±0	±0	±0	±0	±0	±0	±0	±0	±0
T1B2S1	±0	±0	53.7	±0	±0	±0	±0	106.5	±0	±0
T1B2S2	±0	±0	±0	±0	±0	±0	±0	±0	±0	±0
T1B2S3	±0	±0	±0	±0	±0	±0	±0	±0	±0	±0
T1B3S1	68.4	±0	±0	±0	8.7	±0	34.4	±0	±0	±0
T1B3S2	86.5	±0	±0	±0	7.1	±0	±0	±0	±0	±0
T1B3S3	78.1	±0	±0	±0	7.9	±0	±0	±0	±0	±0

Table C.8: Trace element data of the ground- and pore water of Noordwijk. ±0 means that the concentration was below detection limit. The data is incomplete.

Sample	Cu	Zn	Sr	Y	Zr	Mo	Cd	Ba	Pb	U
GW	μg/kg	μg/kg	μg/kg	μg/kg	μg/kg	μg/kg	μg/kg	μg/kg	μg/kg	μg/kg
T1B1	±0	±0	314	±0	±0	±0	±0	34.0	±0	16.4
T1B2	±0	±0	390	±0	±0	±0	±0	±0	±0	16.5
T1B3	±0	137.2	4132	±0	±0	±0	±0	7.1	±0	16.9
T2B1	±0	±0	478	±0	±0	±0	±0	58.6	±0	16.3
T2B2	±0	±0	4115	±0	±0	±0	±0	6.8	±0	17.0
T2B3	±0	±0	5115	±0	±0	±0	±0	9.6	±0	17.0
T3B1	±0	±0	546	±0	±0	±0	±0	9.3	±0	17.9
T3B2	±0	±0	3867	±0	±0	±0	±0	9.1	±0	16.4
T3B3	±0	18.9	5053	±0	±0	±0	±0	8.2	±0	17.1
PW										
T1B1S3	±0	±0	246	±0	±0	±0	±0	±0	±0	±0
T1B1S4	±0	±0	490	±0	±0	±0	±0	±0	±0	±0
T1B2S1	±0	±0	101	±0	±0	±0	±0	±0	±0	±0
T1B2S2	±0	±0	274	±0	±0	±0	±0	±0	±0	±0
T1B2S3	±0	±0	358	±0	±0	±0	±0	±0	±0	±0
T1B3S1	±0	±0	4879	±0	±0	±0	±0	±0	±0	±0
T1B3S2	±0	±0	5306	±0	±0	±0	±0	±0	±0	±0
T1B3S3	±0	±0	5087	±0	±0	±0	±0	±0	±0	±0

Table C.9: Trace element data of the ground- and pore water of IJmuiden. ±0 means that the concentration was below detection limit.

Sample	Li	Be	Al	Sc	V	Cr	Mn	Fe	Co	Ni
GW	μg/kg	μg/kg	μg/kg	μg/kg	μg/kg	μg/kg	μg/kg	μg/kg	μg/kg	μg/kg
T1B1	±0	±0	73.3	±0	69.0	±0	±0	±0	±0	±0
T1B2	39.3	±0	±0	±0	16.2	±0	±0	±0	±0	±0
T1B3	29.9	±0	±0	±0	±0	±0	±0	±0	±0	±0
T2B1	±0	±0	±0	±0	±0	±0	±0	±0	±0	±0
T2B2	±0	±0	±0	±0	±0	±0	±0	±0	±0	±0
T2B3	33.2	±0	±0	±0	±0	±0	±0	±0	±0	±0
T3B1	±0	±0	±0	±0	±0	±0	±0	±0	±0	±0
T3B2	±0	±0	±0	±0	±0	±0	59.6	±0	±0	±0
T3B3	±0	±0	±0	±0	±0	±0	733.9	±0	±0	±0
T4B1	±0	±0	224.8	±0	±0	±0	±0	182.4	±0	±0
T4B2	±0	±0	±0	±0	±0	±0	±0	±0	±0	±0
T4B3	18.9	±0	±0	±0	±0	±0	258.8	268.3	±0	±0
PW										
T1B1S2	±0	±0	129.8	±0	±0	±0	±0	70.7	±0	±0
T1B1S3	±0	±0	48.7	±0	±0	±0	±0	±0	±0	±0
T1B1S4	±0	±0	±0	±0	±0	±0	±0	±0	±0	±0
T1B2S1	±0	±0	274.2	±0	±0	±0	74.9	218.7	±0	66.4
T1B2S2	29.9	±0	±0	±0	6.5	±0	±0	±0	±0	±0
T1B2S3	28.9	±0	±0	±0	±0	±0	±0	±0	±0	±0
T1B3S2	±0	±0	±0	±0	±0	±0	±0	±0	±0	±0
T1B3S3	38.1	±0	±0	±0	±0	±0	±0	±0	±0	±0
T1B4S1	67.4	±0	±0	±0	8.3	±0	±0	±0	±0	±0
T1B4S2	59.8	±0	±0	±0	7.5	±0	±0	±0	±0	±0
T1B4S3	82.1	±0	28.2	±0	8.0	±0	36.7	±0	±0	±0
T3B1S1	±0	±0	±0	±0	±0	±0	±0	±0	±0	±0
T3B1S2	±0	±0	±0	±0	±0	±0	±0	±0	±0	±0
T3B1S3	±0	±0	±0	±0	±0	±0	±0	±0	±0	±0
T3B2S1	±0	±0	±0	±0	±0	±0	±0	±0	±0	±0
T3B2S2	±0	±0	44.6	±0	±0	±0	±0	±0	±0	±0
T3B2S3	±0	±0	289.7	±0	±0	±0	±0	308.3	±0	±0
T3B3S1	±0	±0	±0	±0	±0	±0	±0	±0	±0	±0
T3B3S2	±0	±0	±0	±0	±0	±0	309.9	±0	±0	±0
T3B4S1	74.8	±0	±0	±0	6.4	±0	±0	±0	±0	±0
T3B4S2	79.4	±0	±0	±0	8.4	±0	±0	±0	±0	±0
T3B4S3	89.3	±0	±0	±0	16.9	±0	±0	±0	±0	±0
T4B1S1	±0	±0	±0	±0	±0	±0	±0	±0	±0	±0
T4B1S2	±0	±0	±0	±0	±0	±0	±0	±0	±0	±0
T4B1S3	±0	±0	±0	±0	±0	±0	±0	±0	±0	±0
T4B1S4	±0	±0	±0	±0	±0	±0	±0	±0	±0	±0

Table C.10: Trace element data of the ground- and pore water of IJmuiden as measured by the ICP-MS. ±0 means that the concentration was below detection limit.

Sample	Cu	Zn	Sr	Y	Zr	Mo	Cd	Ba	Pb	U
GW	μg/kg	μg/kg	μg/kg	μg/kg	μg/kg	μg/kg	μg/kg	μg/kg	μg/kg	μg/kg
T1B1	±0	±0	81	±0	±0	±0	±0	7.8	±0	14.3
T1B2	±0	±0	2511	±0	±0	±0	±0	62.3	±0	13.3
T1B3	±0	16.9	2148	±0	±0	±0	±0	18.9	±0	12.6
T2B1	±0	±0	1221	±0	±0	±0	±0	29.5	±0	12.9
T2B2	±0	±0	905	±0	±0	±0	±0	11.6	±0	12.8
T2B3	±0	±0	3040	±0	±0	±0	±0	16.7	±0	13.0
T3B1	±0	±0	166	±0	±0	±0	±0	13.7	±0	12.8
T3B2	±0	±0	150	±0	±0	±0	±0	13.8	±0	13.2
T3B3	±0	±0	1102	±0	±0	±0	±0	8.2	±0	13.0
T4B1	±0	±0	74	±0	±0	±0	±0	6.4	±0	13.6
T4B2	±0	±0	30	±0	±0	±0	±0	43.1	±0	14.5
T4B3	±0	±0	1349	±0	±0	±0	±0	9.1	±0	13.4
PW										
T1B1S2	±0	71.5	61	±0	±0	±0	±0	±0	±0	±0
T1B1S3	±0	±0	26	±0	±0	±0	±0	±0	±0	±0
T1B1S4	±0	±0	39	±0	±0	±0	±0	±0	±0	±0
T1B2S1	±0	44.6	340	±0	±0	±0	±0	±0	±0	±0
T1B2S2	±0	±0	2274	±0	±0	±0	±0	±0	±0	±0
T1B2S3	±0	±0	2343	±0	±0	±0	±0	±0	±0	±0
T1B3S2	±0	±0	1756	±0	±0	±0	±0	±0	±0	±0
T1B3S3	±0	±0	3131	±0	±0	±0	±0	±0	±0	±0
T1B4S1	±0	±0	3661	±0	±0	±0	±0	±0	±0	±0
T1B4S2	±0	±0	3564	±0	±0	±0	±0	±0	±0	±0
T1B4S3	±0	±0	4174	±0	±0	32.1	±0	±0	±0	±0
T3B1S1	±0	±0	130	±0	±0	±0	±0	±0	±0	±0
T3B1S2	±0	±0	171	±0	±0	±0	±0	±0	±0	±0
T3B1S3	±0	±0	177	±0	±0	±0	±0	±0	±0	±0
T3B2S1	±0	±0	152	±0	±0	±0	±0	±0	±0	±0
T3B2S2	±0	±0	111	±0	±0	±0	±0	±0	±0	±0
T3B2S3	±0	±0	52	±0	±0	±0	±0	±0	±0	±0
T3B3S1	±0	±0	563	±0	±0	±0	±0	±0	±0	±0
T3B3S2	±0	±0	526	±0	±0	±0	±0	±0	±0	±0
T3B4S1	±0	±0	4987	±0	±0	±0	±0	±0	±0	±0
T3B4S2	±0	±0	5369	±0	±0	±0	±0	±0	±0	±0
T3B4S3	±0	±0	5187	±0	±0	±0	±0	±0	±0	±0
T4B1S1	±0	32.7	121	±0	±0	±0	±0	±0	±0	±0
T4B1S2	±0	±0	220	±0	±0	±0	±0	±0	±0	±0
T4B1S3	±0	±0	214	±0	±0	±0	±0	±0	±0	±0
T4B1S4	±0	±0	272	±0	±0	±0	±0	±0	±0	±0

Table C.11: Element data as measured by the ICP-OES of the Sand Motor. ±0 means that the concentration was below detection limit. ±62.7 indicates that the concentration is below the BEC (Background Equivalent Concentration), which means that the measurement can have an error of ≥10%. ≥5580 means that the measurement underestimates the actual concentration.

Sample	Al	B	Ca	Cl	Fe	K	Mg
GW	mg/kg	mg/kg	mg/kg	mg/kg	mg/kg	mg/kg	mg/kg
B1	±0	1.7	145.9	≥ 5580	±0.1	129	365
B2	±0	±0.6	58.5	±63	±0.1	34	32
B3	±0	±0.9	106.6	2033	±0.1	64	129
B4	±0	±1.1	15.3	±54	±0.1	37	18
B5	±0	2.3	156.0	≥ 7252	±0.1	184	464
B6	±0	±0.5	42.3	±32	±0.1	36	29.
B7	±0	2.2	225.7	≥ 9660	±0.2	228	667
B8	±0	2.6	253.7	≥ 11039	±0.1	272	772
B9	±0	1.9	223.8	≥ 8310	±0.3	206	585
B10	±0	±0.8	36.9	±63	±0.3	44	46
Lake	±0	2.1	178.6	≥ 7405	±0.1	175	500
Slufter	±0	3.2	314.9	≥ 14180	±0.1	352	1076
PW							
B1S1	±0	2.6	203.7	8480	1.1	198	533.8
B1S2	±0	2.9	194.5	8287	1.1	198	526.8
B2S1	±0.5	±0.4	37.4	±0	3.5	±19	16.9
B2S2	±0	±0.2	44.2	±0	1.4	±12	12.6
B2S3	±0	±0.4	46.2	±0	1.1	±26	18.4
B2S4	±0	1.2	253.7	±0	1.1	46	12.5
B3S1	±0	±0.3	22.5	±0	1.2	±29	9.0
B3S2	±0	±0.7	6.8	±0	2.2	±14	0.7
B3S4	±0	1.1	56.0	1336	1.1	70	57.3
B4S1	±0	±0.2	24.9	±0	1.0	±13	9.7
B4S2	±0	±0.6	31.4	±0	1.1	±22	13.1
B4S3	±0	±0.4	26.3	±157.73	1.1	±26	17.6
B4S4	±0	±0.9	18.2	±0	1.2	51	16.3
B5S1	±0	3.7	265.6	≥ 14387	1.1	359	891.1
B5S2	±0	4.2	319.2	≥ 14754	1.1	363	982.6
B5S3	±0	4.0	312.2	≥ 14790	1.1	353	956.9
B8S1	±0	4.3	328.5	≥ 15171	1.1	374	999.9
B8S2	±0	4.1	342.4	≥ 15237	1.1	363	997.9
B9S1	±0	3.2	56.3	3199	1.4	109	81.5
B9S2	±0	3.1	172.2	7964	1.1	213	463.0
B9S3	±0	2.4	202.1	7788	1.1	214	497.1
B10S2	±0.6	±0.4	30.9	±0	1.9	±25	11.5
B10S3	±0	±0.5	90.4	±0	1.2	35	32.6
B10S4	±0	±0.9	34.8	±0	1.1	62	36.4

Table C.12: Element data as measured by the ICP-OES of the Sand Motor. ±0 means that the concentration was below detection limit. ±62.7 indicates that the concentration is below the BEC (Background Equivalent Concentration), which means that the measurement can have an error of ≥10%. ≥5580 means that the measurement underestimates the actual concentration.

Sample	Na	P	S	Si	Ti	Zr
GW	mg/kg	mg/kg	mg/kg	mg/kg	mg/kg	mg/kg
B1	≥3626	±0	≥189	±1.3	±0	±0.01
B2	93.7	±0	43.0	3.2	±0	±0.01
B3	≥1852	±0	≥132	3.3	±0	±0.01
B4	120.9	±0	27.1	3.4	±0	±0.01
B5	≥3633	±0	≥207	1.8	±0	±0.01
B6	44.6	±0	31.6	4.4	±0	±0.01
B7	≥3596	±0	≥204	±1.3	±0	±0.01
B8	≥3580	±0	≥186	±0.9	±0	±0.01
B9	≥3624	±0	≥209	±1.5	±0	±0.01
B10	93.4	±0	47.4	4.6	±0	±0.01
Lake	≥3632	±0	≥206	±0.2	±0	±0.01
Slufter	≥3584	±0	≥86	±0.4	±0	±0.01
PW						
B1S1	≥5382	±0	407.9	2.0	±0	±0.06
B1S2	≥5241	±0	405.1	2.0	±0	±0.06
B2S1	60.3	±0	40.9	3.6	±0	±0.06
B2S2	30.9	±0	19.2	3.3	±0	±0.07
B2S3	43.7	±0	29.2	3.2	±0	±0.06
B2S4	187.3	±0	45.6	3.7	±0	±0.06
B3S1	68.6	±0	23.0	3.1	±0	±0.06
B3S2	212.2	±0	15.1	4.5	±0	±0.08
B3S4	956.0	±0	114.3	4.1	±0	±0.06
B4S1	22.9	±0	10.3	5.6	±0	±0.05
B4S2	61.5	±0	27.9	4.7	±0	±0.06
B4S3	29.7	±0	12.7	4.8	±0	±0.06
B4S4	85.4	±0	22.2	3.9	±0	±0.07
B5S1	≥11051	±0	≥693	±1.1	±0	±0.06
B5S2	≥10912	±0	≥700	±1.3	±0	±0.06
B5S3	≥10693	±0	≥696	±1.4	±0	±0.06
B8S1	≥11271	±0	≥713	±1.2	±0	±0.06
B8S2	≥11291	±0	≥732	1.9	±0	±0.06
B9S1	1990.0	±0	160.6	3.0	±0	±0.06
B9S2	≥4962	±0	370.4	2.2	±0	±0.06
B9S3	≥4953	±0	382.9	2.5	±0	±0.06
B10S2	35.3	±0	19.9	3.7	±0	±0.07
B10S3	58.3	±0	143.3	3.0	±0	±0.06
B10S4	80.8	±0	49.1	4.5	±0	±0.07

Table C.13: Element data as measured by the ICP-OES of Noordwijk. ±0 means that the concentration was below detection limit. ±62.7 indicates that the concentration is below the BEC (Background Equivalent Concentration), which means that the measurement can have an error of ≥10%. ≥5580 means that the measurement underestimates the actual concentration.

Sample	Al	B	Ca	Cl	Fe	K	Mg
GW	mg/kg	mg/kg	mg/kg	mg/kg	mg/kg	mg/kg	mg/kg
NW T1B1	±0	±0.5	38.5	272	±0.1	±21	39
NW T1B2	±0	±1.0	25.9	1242	±0.1	42	70
NW T1B3	±0	2.7	252.1	≥11467	±0.1	287	814
NW T2B1	±0	±0.4	59.5	±163	±0.1	±14	31
NW T2B2	±0	2.5	≥243	±0	±0.1	≥215	≥596
NW T2B3	±0	3.1	321.5	±0	±0.1	369	1117
NW T3B1	±0	±0.5	51.4	±172	±0.1	±17	30
NW T3B2	±0	2.5	252.3	≥11345	±0.1	274	782
NW T3B3	±0	3.2	318.8	≥14567	±0.1	364	1109
PW							
NW T1B1S3	±0	±0.5	22.8	220	1.1	±31	26
NW T1B1S4	±0	±0.5	57.5	258	1.1	±20	41
NW T1B2S1	±0	2.2	10.5	617	1.3	43	14
NW T1B2S2	±0	2.6	19.8	1495	1.1	62	44
NW T1B2S3	±0	1.4	23.5	1147	1.0	57	62
NW T1B3S1	±0	3.9	305.7	≥13832	1.1	343	893
NW T1B3S2	±0	3.9	307.5	≥14063	1.2	342	936
NW T1B3S3	±0	3.8	314.9	≥14424	1.1	345	954

Table C.14: Element data as measured by the ICP-OES of the Noordwijk. ±0 means that the concentration was below detection limit. ±62.7 indicates that the concentration is below the BEC (Background Equivalent Concentration), which means that the measurement can have an error of ≥10%. ≥5580 means that the measurement underestimates the actual concentration.

Sample	Na	P	S	Si	Ti	Zr
GW	mg/kg	mg/kg	mg/kg	mg/kg	mg/kg	mg/kg
NW T1B1	177.5	±0.06	24.7	2.7	±0	±0.01
NW T1B2	≥1051	±0.1	≥71	±1.1	±0	±0.01
NW T1B3	≥3578	±0	≥185	±1.0	±0	±0.01
NW T2B1	125.5	±0.02	16.7	3.5	±0	±0.01
NW T2B2	≥3578	±0	≥180	±1.0	±0	±0.01
NW T2B3	≥3582	±0	≥112	±0.8	±0	±0.01
NW T3B1	138.7	±0	18.4	2.7	±0	±0.01
NW T3B2	≥3581	±0	≥192	±0.8	±0	±0.01
NW T3B3	≥3585	±0	≥90	±0.9	±0	±0.01
PW						
NW T1B1S3	152.3	±0	14.7	3.1	±0	±0.06
NW T1B1S4	145.7	±0	19.5	4.6	±0	±0.06
NW T1B2S1	528.9	±0	35.4	3.4	±0	±0.06
NW T1B2S2	1097.4	±0	84.8	2.3	±0	±0.06
NW T1B2S3	762.6	±0	63.9	2.3	±0	±0.05
NW T1B3S1	≥9814	±0	≥653	2.0	±0	±0.07
NW T1B3S2	≥10029	±0	≥677	1.8	±0	±0.06
NW T1B3S3	≥10154	±0	≥683	2.0	±0	±0.07

Table C.15: Element data as measured by the ICP-OES of IJmuiden. ±0 means that the concentration was below detection limit. ±62.7 indicates that the concentration is below the BEC (Background Equivalent Concentration), which means that the measurement can have an error of ≥10%. ≥5580 means that the measurement underestimates the actual concentration.

Sample	Al	B	Ca	Cl	Fe	K	Mg
GW	mg/kg	mg/kg	mg/kg	mg/kg	mg/kg	mg/kg	mg/kg
IJ T1B1	±0.19	2.0	7.9	460	±0.2	±24.0	12.8
IJ T1B2	±0	1.2	179.9	≥6420	±0.1	140	440.8
IJ T1B3	±0	1.7	185.0	≥5634	±0.1	144	366.0
IJ T2B1	±0	±1.0	145.8	1914	±0.1	59	155.7
IJ T2B2	±0	1.8	79.8	2256	±0.1	74	147.0
IJ T2B3	±0	1.6	243.0	≥8164	±0.1	190	593.4
IJ T3B1	±0	±0.6	19.1	228	±0.1	±31.7	27.7
IJ T3B2	±0	±0.5	17.4	368	±0.1	±26.4	25.9
IJ T3B3	±0	±0.6	95.3	2794	±0.1	57	173.5
IJ T4B1	±0.2	±0.4	9.3	±62	±0.4	±14.7	8.3
IJ T4B2	±0	1.2	3.4	±145	±0.1	±14.2	5.9
IJ T4B3	±0	1.2	101.3	3925	±0.5	112	294.4
PW							
IJ T1B1S1	±0	±1.0	28.2	268	1.5	36	17.5
IJ T1B1S2	±0	2.8	12.1	218	1.1	±24.7	6.3
IJ T1B1S3	±0	1.8	4.1	±0	1.2	±18.4	2.8
IJ T1B1S4	±0	2.5	4.4	217	1.1	±25.6	5.9
IJ T1B2S1	±0.6	2.2	30.5	1390	1.4	58	47.8
IJ T1B2S2	±0	2.0	169.4	6379	1.1	169	380.3
IJ T1B2S3	±0	1.9	185.1	6694	1.1	162	397.9
IJ T1B3S1	±0	±1.0	48.1	±0	2.6	57	27.8
IJ T1B3S2	±0	1.4	155.4	5687	1.1	131	317.9
IJ T1B3S3	±0	1.9	250.9	5935	1.2	172	404.4
IJ T1B4S1	±0	3.4	261.0	≥14020	1.0	359	852.1
IJ T1B4S2	±0	3.2	261.7	≥12286	1.1	317	783.0
IJ T1B4S3	±0	3.2	272.0	≥12459	1.1	369	775.2
IJ T3B1S1	±0	±0.7	17.0	±198	1.1	40	17.2
IJ T3B1S2	±0	±0.5	20.4	±0	1.1	±32.12	22.2
IJ T3B1S3	±0	±0.6	21.7	±0	1.1	±26.1	19.8
IJ T3B2S1	±0	±0.3	18.8	±0	1.1	±32.1	21.7
IJ T3B2S2	±0	±0.4	13.5	±0	1.2	36	14.9
IJ T3B2S3	±0.6	±0.6	7.5	±0	1.4	±21.7	7.6
IJ T3B3S1	±0	±0.8	52.3	980	1.1	41	44.0
IJ T3B3S2	±0	±0.9	38.5	1704	1.1	57	70.6
IJ T3B4S1	±0	4.0	313.9	≥14304	1.1	351	946.0
IJ T3B4S2	±0	4.3	342.5	≥15556	1.1	391	1019.0
IJ T3B4S3	±0	4.3	332.7	≥15389	1.1	404	999.6
IJ T4B1S1	±0	±0.5	17.4	±0	1.1	±23.2	19.0
IJ T4B1S2	±0	±0.4	23.3	±0	1.1	±26.1	22.1
IJ T4B1S3	±0	±0.4	24.4	±0	1.1	36	20.3
IJ T4B1S4	±0	±0.6	27.5	±193	1.1	38	25.9

Table C.16: Element data as measured by the ICP-OES of the IJmuiden. ±0 means that the concentration was below detection limit. ±62.7 indicates that the concentration is below the BEC (Background Equivalent Concentration), which means that the measurement can have an error of ≥10%. ≥5580 means that the measurement underestimates the actual concentration.

Sample	Na	P	S	Si	Ti	Zr
GW	mg/kg	mg/kg	mg/kg	mg/kg	mg/kg	mg/kg
IJ T1B1	≥669	1.6	49.1	2.1	±0	±0.01
IJ T1B2	≥3620	±0.06	≥195	±1.0	±0	±0.01
IJ T1B3	≥3627	±0	≥186	±1.5	±0	±0.01
IJ T2B1	≥1336	±0.04	≥88	3.2	±0	±0.01
IJ T2B2	≥1952	±0.25	≥115	1.7	±0	±0.01
IJ T2B3	≥3623	±0	≥209	±1.47	±0	±0.01
IJ T3B1	192.2	±0.22	24.4	2.7	±0	±0.01
IJ T3B2	≥248	±0.19	15.6	±1.1	±0	±0.01
IJ T3B3	≥2288	±0.02	≥113	±1.3	±0	±0.01
IJ T4B1	90.6	1.1	6.5	2.1	±0.01	±0.01
IJ T4B2	≥262	1.2	12.9	±1.47	±0	±0.01
IJ T4B3	≥3250	±0.69	≥147	1.9	±0	±0.01
PW						
IJ T1B1S1	123.6	±0	17.4	4.7	±0	±0.08
IJ T1B1S2	355.8	1.1	22.2	2.4	±0	±0.05
IJ T1B1S3	291.8	1.1	13.7	2.8	±0	±0.06
IJ T1B1S4	429.8	±0	21.8	2.9	±0	±0.07
IJ T1B2S1	1035.7	±0	113.7	2.4	±0	±0.06
IJ T1B2S2	≥3895	±0	274.2	1.8	±0	±0.06
IJ T1B2S3	≥4148	±0	310.2	2.3	±0	±0.06
IJ T1B3S1	102.1	±0	11.7	5.1	±0	±0.14
IJ T1B3S2	≥3410	±0	278.5	1.8	±0	±0.07
IJ T1B3S3	≥3324	±0	294.7	2.7	±0	±0.07
IJ T1B4S1	≥10637	±0	≥662	±1.0	±0	±0.06
IJ T1B4S2	≥8622	±0	≥601	±1.47	±0	±0.06
IJ T1B4S3	≥8930	±0	≥614	±1.2	±0	±0.06
IJ T3B1S1	117.0	±0	10.0	4.0	±0	±0.06
IJ T3B1S2	98.4	±0	13.2	4.0	±0	±0.06
IJ T3B1S3	83.3	±0	9.5	3.9	±0	±0.07
IJ T3B2S1	35.5	±0	±3.1	3.4	±0	±0.06
IJ T3B2S2	50.8	±0	±0	2.8	±0	±0.06
IJ T3B2S3	183.4	±0	6.9	2.7	±0	±0.06
IJ T3B3S1	589.6	±0	40.2	±1.5	±0	±0.07
IJ T3B3S2	1132.1	±0	87.1	2.3	±0	±0.06
IJ T3B4S1	≥10270	±0	≥672	1.6	±0	±0.06
IJ T3B4S2	≥11522	±0	≥723	1.9	±0	±0.06
IJ T3B4S3	≥11393	±0	≥728	1.9	±0	±0.06
IJ T4B1S1	25.5	±0	±3.0	3.6	±0	±0.06
IJ T4B1S2	24.6	±0	±0	3.5	±0	±0.06
IJ T4B1S3	42.1	±0	±4.3	3.3	±0	±0.06
IJ T4B1S4	124.3	±0	16.2	3.6	±0	±0.06